UNIVERSITAT POLITÈCNICA
DE CATALUNYA
BARCELONATECH

UPCommons

Portal del coneixement obert de la UPC

http://upcommons.upc.edu/e-prints

Aquesta és una còpia de la versió *author's final draft* d'un article publicat a la revista: Composites. Part A, applied science and manufacturing.

URL d'aquest document a UPCommons E-prints:
http://hdl.handle.net/2117/112020

Article publicat / *Published paper*:

Gomez, J., Sanchez-Soto, M., Maspoch, M. (2018) Microcellular PP/GF composites: morphological, mechanical and fracture characterization. "Composites. Part A, applied science and manufacturing", vol. 104, p. 1-13. Doi: 10.1016/j.compositesa.2017.10.014

*Manuscript
Click here to view linked References

Microcellular PP/GF composites: Morphological, mechanical and fracture characterization

J. Gómez-Monterde[a,*], M. Sánchez-Soto[b], M. Ll. Maspoch[b]

[a]SEAT SA. Autovía A-2, km 585. Apartado de correos 91, E-08760 Martorell, Spain.

[b]Centre Català del Plàstic, Universitat Politècnica de Catalunya-BarcelonaTech (ETSEIB, ETSEIAT). Carrer Colom 114, E-08222 Terrassa, Spain.

*Corresponding author:

Javier Gómez-Monterde (E-mail: javier.gomez@upc.edu / Telephone: +34 93 7731113)

ABSTRACT

The aim of the present work is to analyze the morphology, mechanical properties and fracture behaviour of solid and foamed plates made of glass fiber-reinforced PP. The morphology exhibited a solid skin/foamed core structure, dependent on the foaming ratio. Simulation of the microcellular injection molding process with *Moldex 3D®* software provided a good approach to the experimental results. The flexural properties and impact resistance showed lower values as the apparent density decreased, but constant specific properties. The fracture characterization was carried out by determining the *Crack Tip Opening Displacement* (*CTOD*) at low strain rate, as well as the fracture toughness (K_{Ic}) at impact loading. Foamed specimens presented higher values of *CTOD* than the solid ones and higher as the foaming ratio increases, due to cells acting as crack arrestors by blunting the crack tip. However, the fracture toughness K_{Ic} decreased with decreasing the apparent density. Anisotropy due to fiber orientation was also observed. Fibers were aligned in the filling direction in the surface layers, while they were oriented in the transverse direction in the core. According to the amount of fibers oriented in one direction or another, different properties were obtained.

KEYWORDS: Foams; Polymer-matrix composites (PMCs); Fracture toughness; Injection moulding.

INTRODUCTION

The relative low material density and cost, easy processing and good mechanical properties of Polypropylene (PP) make it suitable for a wide range of applications. PP is widely used in automotive parts either in the form of homopolymer or copolymer with enhanced impact resistance [1]. The demand for lighter constructions and reductions in fuel consumption and greenhouse gas emissions [2] makes PP foams potentially interesting for automotive products.

Foamability of PP has been extensively studied by the way of batch methods [3], extrusion [4] and injection molding processes [5]. Unfortunately, the low melt strength of PP and its crystalline nature results in poor cell structure [6]. Low solubility and diffusivity of blowing agents in PP have been determined [7], leading to inhomogeneous morphology along the part. On the other hand, the weak melt strength promotes cell walls breakage under elongational forces while processing, causing cell coalescence, open-cell structures and decrease of mechanical properties [8].

Different methods have been conducted aimed to improve cell nucleation behavior and melt strength of PP, such as long-chain branching [9], ramified molecular structures [8, 10] and blending with other polymer [11]. Furthermore, it has been reported that inorganic fillers dramatically enhance cell structure of foamed polymers acting as nucleating agents. Leung, Wong *et al* [12] showed that additives with many crevices of small semiconical angles lead to higher quality polymer foams, with a high cell density, a smaller cell size and narrower cell size distribution. Some of the most common fillers, namely talc, calcium carbonate, silica and carbon fibers have been successfully employed to the formation of fine and uniform cell morphologies [13, 14], as well as wood fibers, clay and rubber particles [15-18]. Among the different fillers, glass fibers (GF) are the most common reinforcement for polymeric matrix composites, having an excellent relationship between low cost, high stiffness and strength, high chemical resistance, and insulating properties, but with the disadvantages of low tensile modulus, relatively high specific gravity, sensitivity to abrasion during handling, low fatigue resistance and high hardness [19]. They have been traditionally utilized in many industrial applications due to the increase in stiffness and strength of reinforced thermoplastics, creep resistance and service temperature. Regarding foaming experiments with PP/GF composites, Xi, Sha *et al* [20] determined an optimum fiber content of 11.8% for improving cell morphology and mechanical properties.

The fracture toughness and *J-integral* of discontinuous glass fiber mat reinforced polypropylene was studied under static and dynamic conditions by Benevolenski and Karger-Kocsis [21]. It was also demonstrated the increase of PP resistance against stable crack propagation as the crystallinity degree raises [22]. Due to the ductile nature of PP material, fracture behavior of solid and foamed PP has been mostly studied by means of the concept of *Essential Work of Fracture* (*EWF*) [23, 24]. This method has been also successfully applied for PP/GF systems based on the energy partitioning concept [25]. However, the fracture characterization of PP/GF foamed composites is more difficult and has not been widely researched yet, because of their multiphasic composition, more complex failure modes and anisotropic behavior. The objective of the present work is to analyze the morphology, mechanical properties and fracture behavior of PP/GF composites foamed by the microcellular injection molding *MuCell®* technology, with the purpose of obtaining lightweight composites suitable for industrial applications, like automotive.

MATERIALS AND METHODS

Material

In this project a 20% chemically coupled high performance Glass Fiber reinforced Polypropylene compound (PP 20GF *Fibremod™ GE277Al*) was employed. It is supplied by *Borealis AG* (Austria), with a density of 1.04 g cm^{-3} (ISO 1183) and a melt flow index of 12 g 10 min^{-1} (ISO 1133).

Injection molding

Square plates of 100x100x5 mm^3 (Figure 1) were injection molded in a Victory 110 injection molding machine (*Engel GmbH*, Germany), with a clamping force of 1100 kN and equipped with an injection valve II series of 25 mm, the *MuCell®* (*Trexel Inc.*, USA) supercritical fluid (*SCF*) supply system and a shut-off nozzle developed for such system. As recommended by the supplier, the PP 20GF compound was also pre-dried at 80 ºC for a minimum of 3 hours.

Solid and two series of foamed plates with 10% and 20% levels of weight reduction were produced. The shot volume for solid injection moldings was 70 cm^3, while it was 51.2 and 45.3 cm^3 for both levels of foamed plates. In all experiments both the melt temperature profile and cooling time were kept constant. The melt temperature from hopper to nozzle was 190-200-210-225-235 ºC. The cooling time was set to 30 seconds. Solid plates were injection molded at speed of 45 cm^3 s^{-1}, mold temperature of 47 ºC, and a holding pressure of 200 bar that was applied for 15 seconds. Preliminary trials showed that an injection rate of 40 cm^3 s^{-1} and a mold temperature of 35 ºC optimized the morphology and mechanical properties of the foamed samples, with no holding stage. The content of the blowing agent (N_2) was 0.76% for the former series of foamed plates (10% of weight reduction) and 0.86% for the latter (20% of weight reduction).

The microcellular injection molding process of the square plates was simulated with the aid of the *Moldex 3D®* commercial software (*CoreTech System Co.*, Taiwan), in order to compare the results with the experimental ones obtained by the morphological analysis.

Characterization methods

Morphology and apparent density

The morphology of the foamed specimens was analyzed at 10 mm-width cross sections taken at different distances from the injection gate both in a parallel (MD) and transversal direction (TD) to the injection flow (Figure 1a)). Samples were submitted to cryogenic fracture so as to avoid altering the original morphology, and the resulting fracture surfaces were examined by *Scanning Electron Microscopy* (*SEM*) using a *JEOL JSM-560* microscope (*Jeol Ltd.*, Japan). Micrographs were adjusted for an appropriate level of contrast and morphological parameters, such as cell size, cell density and skin thickness were determined with the aid of *Igor Pro®* (*Wavemetrics Inc.*, USA) and *Matlab®* (*The MathWorks Inc.*, USA) software (Figure 3.7). Cell density represents the number of cells per volume (cells cm^{-3}) with respect to the unfoamed solid polymer and it is calculated as follows [26]:

$$N = \left(\frac{n}{A}\right)^{3/2}\left(\frac{\rho_s}{\rho_f}\right) \quad (1)$$

where n is the number of cells in the micrograph, A is the analyzed area (cm^2) and ρ_s and ρ_f are the density of solid and foamed material, respectively. The area of each cell of the micrograph was measured and, assuming all of them were completely spherical, an equivalent cell diameter or cell size was determined. The skin thickness was measured as the distance between the surface and the first cells of the foamed core.

The cell morphology and fiber orientation and distribution of the PP 20GF plates were analyzed by the *Computed Tomography* (*CT*) technique. Samples of 15x15 mm^2 were tooled from the plates at the same positions as those examined by *SEM* and scanned with a micro-computerized tomography *MultiTom Core* system, (*XRE bvba*, Belgium). The samples were scanned at tube conditions of 90kV and 10W, for a total of 2500 projections and an exposure time of 400 ms, resulting in a mean scan duration of 22 minutes and obtaining a voxel size resolution of 6 µm. All data from each sample was 3D reconstructed and filtered and, finally, segmentation of materials depending on its density, i.e. fibers, polymer and air, was carried out using *Avizo* software (*FEI Company*, USA).

The content of glass fiber reinforcement in the PP 20GF samples was carried out by the determination of ash through the direct calcination method, following the guidelines set by the ISO 3451-1 standard. The apparent density was calculated by measuring and weighing specimens extracted from the injected plates at the same positions as the ones analyzed by *SEM* method.

Mechanical properties

The mechanical properties of solid and foamed samples were assessed through flexural and impact tests. For all materials and types of tests, the specimens were machined out of the plates according to the schemes shown in Figure 1b), ensuring the correspondence between the tested section and the morphology previously analyzed. At least five samples of solid and foamed materials were tested under room temperature for each position and direction.

Flexural tests were carried out in 100x10 mm^2 (length x width) specimens. Experiments were done following the ISO 178 standard, in a *Galdabini Sun 2500* (*Galdabini SPA*, Italy) testing machine equipped with a 5 kN load cell, at a crosshead speed of 10 mm min^{-1}, and a span length of 80 mm.

Charpy impact tests were made on 80x10 mm^2 (length x width) unnotched samples in flatwise configuration (Figure 1b)). The impact tests were carried out using an instrumented *Ceast Resil* impactor (*Instron Ltd.*, UK), equipped with a 15J hammer. It was impacted at an angle of 99º, resulting in an impact rate of 2.91 m s^{-1}. The span length was 62 mm. Force, displacement, energy and time values were recorded by a data acquisition system *DAS-1600* from *Ceast*.

Fracture behavior

The fracture behavior of the solid and foamed square plates was characterized at low loading speed by the *Crack Tip Opening Displacement* (*CTOD*), as well as at high testing rate by the fracture toughness (K_{Ic}). In order to relate the fracture properties with the cell structure determined by morphology analysis, the same distances from the injection gate and orientations were employed. It is worth to notice that for fracture analysis the mold filling and notching directions are transversal to each other. That is, a sample cut-off along the mold flow (MD) has the notch and crack propagation in the transverse direction (TD). To avoid confusion in this point, the samples of the present work have been coded only according to the crack propagation direction (Figure 1c)). All fracture tests were performed at room temperature and the notch was sharpened by sliding a razor blade. At least five specimens were tested for each material, orientation and loading speed.

SENT (*Single Edge Notched Tension*) specimens were employed to determine the *CTOD* parameter, whose size and dimensions are plotted in Figure 1c). The notch length/width ratio (*a/b*) was kept at 0.6, in order to avoid triaxial stress states at the crack tip [27]. The low speed tests were performed using a *Zwick/Roell* universal testing machine, *Amsler HC25/200*8 model (*Zwick GmbH & Co. KG*, Germany), at a crosshead rate of 16 mm min^{-1}. The tests were recorded by two digital cameras at a frame rate of 10 pictures per second (*Xenoplan 1.4/23-0.902*, *Schneider Optische Werke GmbH*, Germany) coupled to a *GOM/ARAMIS* (*GOM mbH*, Germany) *Digital Image Correlation* system (*DIC*). The *CTOD* parameter was calculated by measuring the displacement of the notch faces in the notch root, at the crack propagation onset.

The fracture toughness of the solid and foamed plates was assessed through *SENB* (*Single Edge Notched Bending*) specimens, as shown in Figure 1c). According to the testing protocol for determining fracture toughness at moderately high loading rates [28], the a/b ratio was in the range of $0.45 \leq a/b \leq 0.55$. The impact tests at 1 m s^{-1} were carried out using an instrumented *Ceast Resil* impactor (*Instron Ltd.*, UK), equipped with a 15J hammer. The pendulum had a length of 0.374 m and a reduced mass of 3.654 kg, and it was impacted at an angle of 30º. Force, displacement, energy and time were recorded by a data acquisition system *DAS-1600* from *Ceast*. The fracture toughness K_{Ic} (MPa m$^{1/2}$) was calculated as follows:

$$K_{Ic} = f \frac{P_q}{h\sqrt{b}} \qquad (2)$$

Where P_q is the calculation force (N), h and b are the part thickness and width (mm) respectively, and f is a geometric function depending on the *a/b* ratio and determined according to the aforementioned protocol.

RESULTS AND DISCUSSION

Morphology and apparent density

SEM micrographs taken from different sections and visualization directions (MD/TD) of the foamed samples are outlined in Figure 2 and Figure 3. From all of them it can be concluded that the material structure consists of two surface solid layers and a foamed core. It has been reported the difficulties in foaming PP because of its low melt strength and crystalline regions [29]. According to Jiang, Liu *et al* [30], cells nucleate at the centers, boundaries and interlamellar amorphous regions of spherulites of pure PP, resulting in inhomogeneous cell distribution. However, SEM pictures shown in Figure 2 and Figure 3 exhibit uniform cell structure. Hence, it is clear that the governing mechanism for cell nucleation was heterogeneous nucleation induced by glass fiber. According to the classical nucleation theory [31], undissolved gas trapped at the filler/polymer interface promotes the occurrence of multitude of sites for cell formation requiring much lower activation energy for bubble nucleation, accelerating cell nucleation and the development of a large number of cells with small cell size. Moreover, the added fillers increase melt strength of the material [13], contributing to prevent cell coalescence and improving its foaming behavior.

The morphological parameters are summarized in Table 1. On one hand, the solid skin becomes thicker as the distance from the injection gate increases (MD-A < MD-B < MD-C), due to the fact that the molten polymer reaches the cavity ends at lower temperatures and solidifies faster, preventing the expansion of the foamed core. Due to this build-up in the solid skin thickness, sections at the end of the cavity are denser than those near the injection gate (Table 1). In TD direction, however, the solid skin thickness remained practically constant in all different studied sections (TD-A, TD-B and TD-C) for each condition. Furthermore, this surface layer is thicker in foamed samples with 10% of weight reduction, as compared to that of 20%-reduced weight foams, because of higher expansion of the foamed core with higher contents of blowing agent.

Cell density remains in the order of magnitude of 10^6 cells cm^{-3} in all cases. Previous research works carried out with ABS polymer concluded that the higher gas content would increase cell nucleation, and therefore, the number of cells per volume. However, it has also been highlighted the relative low melt strength of PP material. If the growing force of cells is larger than the strength of cell walls, cell coalescence occurs and results in larger bubbles but similar cell density for both levels of weight reduction. Nevertheless, Figure 4 points out analogous cell size distributions in every analyzed sample, with 90% of them smaller than 100 μm, despite the lighter foamed series contained some bigger cells.

Results obtained from Moldex 3D® simulation experiments are summarized in Figure 5. As previously stated with ABS cylindrical bars, numerical simulation provided comparable results of cell density and cell size to the experimental analysis for all studied sections (Table 1). Although the increase in the amount of blowing agent for foaming with 20% of weight reduction, the software predicted no changes in cell density and slightly lower cell sizes, concurring with the range of bubble diameter that contains around 85% of cells.

On the other hand, Table 1 shows that fiber content is in the range of 20.4 ± 0.2%, being the fiber concentration in solid plates of 20.3 ± 0.2% and 20.5 ± 0.1% in the polymer in pellets form. That is, the filler content remained invariant despite the decrease in apparent density from 1.03 ± 0.03 g cm^{-3} (solid plates) to 0.88 ± 0.01 g cm^{-3} and 0.79 ± 0.01 g cm^{-3} (10% and 20% of weight reduction, respectively) which is only due to the foaming process.

Another important morphological feature of fiber-filled composites is the orientation and distribution of the fibers. In these materials, the orientation of the fibers has more effect on the mechanical response than the molecular orientation [32]. Additionally, it can influence shrinkage and warpage of the part and compromise its dimensional stability. Pictures of fiber orientation in the surface and in the middle plane of the molded samples taken from *Computed Tomography* technique are illustrated in Figure 6. To better understand this phenomenon, the flow pattern (melt front vs. time) obtained from simulation is included. In the center plane of the plates, the flow is divergent and induces transverse alignment of fibers to filling direction due to an elongation effect [33]. On the contrary, near the walls, shear stress causes a higher orientation of glass fibers in the flow direction or, as in this case, no obvious preferential alignment in the surface layers. Since at side and end areas of the plate (TD-A, TD-C and MD-C) the polymer is colder and the shear stress is greater than the elongation efforts, higher amount of fibers oriented in the flow direction as compared to the center and beginning sections of the plates (MD-A, MD-B and TD-C) is expected.

These fiber orientation and distribution patterns are in agreement to the first researches carried out by different authors [34, 35]. According to the type of load and ratios of skin/core at different positions in the molded plates, the mechanical response will be higher or lower in magnitude. Gong, He *et al* [36] discussed about a minimum length of the glass fiber in order to effectively bear stress in foamed PP. From the CT analysis carried out in this work, an average length of 740 ± 150 µm of the glass fibers for all solid and foamed samples was calculated. Since the maximum cell size is about 250 µm, these fibers are long enough to pass through the cells and reinforce the polymer matrix.

Flexural behavior

The stress-strain curves and flexural properties obtained in solid and all foamed samples are plotted on Figure 7 and Table 2. Flexural strength and modulus decrease accordingly with the apparent density, due to the decrease in the solid skin and the effective cross-sectional area. By reducing 10% the weight of the injected plates, the flexural modulus and strength reduces by around 6% and 14% in MD, respectively, whereas it is diminished by 20% and 27% in the opposite orientation. In case of series with 20% of weight reduction, flexural modulus and strength decreases by 16% and 24% in MD, and by 32% and 40% in TD direction. The dependency of the flexural properties with the apparent density can be observed in the specific values summarized in Table 2, where results of solid and foamed specimens were equated or even exceeded. It is well-known that under a bending load the normal stress is maximum at surfaces and null at the neutral axis. Since the foamed nucleus reduces the density of the microcellular part, but there is almost no stress supported in that area, the specific flexural modulus and strength can be the same or higher than that of the solid material.

Glass fiber-filled composites are characterized by a remarked anisotropy [37]. Notwithstanding a preferential fiber orientation in the surface layers could not be clearly determined from the CT pictures of Figure 6, the values of Table 2 evidence a reinforcing effect of fibers favored in the direction of flow at the extreme locations of the plates in the direction of filling (MD-A and MD-C). This allowed keeping enough stiffness to bear the mechanical loads and overcome the loss in flexural properties due to density reduction. The inexistence of open cells also contributed to enhance the flexural properties of foamed samples. In the transversal direction (TD), the highest elastic modulus and strength are determined at the furthest location from the injection gate (TD-C), which is explained by the thicker solid skin and higher apparent density obtained at the end of the cavity.

Regarding anisotropy, differences in modulus and strength of solid samples between MD and TD directions are about 20%, whereas they were about 30% in foamed specimens. However, it must be noticed that solid square plates were injection molded at higher speed and mold temperature than the studied foamed series. It is known that higher fiber orientation in filling direction is produced when injecting at lower speed [19]. Therefore, direct conclusions about anisotropy changes due to foaming cannot be drawn from this study.

A higher isotropic behavior is found in the middle of the injected plates, where flexural properties of both directions (MD-B and TD-B) are closer. Elongation and shear stress are balanced in this region, which suggests a more random fiber orientation in this area.

Impact behavior

Force-displacement curves of solid and foamed specimens are illustrated in Figure 8. It has been reported in the literature that PP becomes brittle with the addition of glass fibers [38]. Thus, the capability of energy absorption becomes lower. According to Thomason [39], the effect of fiber on PP matrix is contradictory. On one hand, regions from fiber-matrix debonding act as critical flaws and reduce the energy required to initiate a crack. On the other, reinforced material is both stiffer and stronger than unfilled material, so the resistance to crack propagation is significantly increased. Moreover, investigations carried out by Yu, Geng *et al* [40] showed that glass fiber promotes extrinsic toughening mechanism increasing the impact resistance of PP matrix.

Impact resistance values are summarized in Table 3. In case of solid samples, this parameter was very similar in all specimens tested through the whole plate, so fiber orientation seems not to be greatly influent on the impact resistance, as it has been found in other studies [41]. A slight decrease in impact resistance as the distance from the injection gate rises is observed (TD-A < TD-B < TD-C), which might be attributed to a lower material packing at the end of the cavity. However, it is noticeable the reduction in impact resistance in samples tested in MD direction in the middle of the plate (MD-B), which has been also observed in flexural properties and could be explained by the random fiber orientation in that location.

Regarding foamed specimens, impact resistance is lowered with decreasing density and solid skin thickness. From results of Table 3, impact resistance decreases by 18% and 27% (10% and 20% of weight reduction) when samples are tested in MD direction, whereas it is reduced by 29% and 47% in the opposite direction. According to Li, Cao *et al* [42], the impact resistance of microcellular foams depends on the material toughness itself and on the effect of foaming. And this effect results from the combination of two opposite mechanisms that exist simultaneously. On one hand, cells can passivate the stress of crack tips, dissipate impact energy and then increase impact strength. On the other hand, the reduction of the effective sectional area and cells collapse decrease the impact resistance. The predominant mechanism of foaming effect for this material seems to be the reduction in resistant area and cells collapse acting as intern defects, thus decreasing the impact resistance.

As said above, processing parameters could led to higher preferential fiber orientation parallel to filling direction in microcellular parts. That is the reason why higher anisotropic behavior is found in foamed specimens. The impact resistance keeps almost constant or slightly increased at the end of the cavities (comparing TD-A, TD-B and TD-C in Table 3), also due to the slight increase in skin thickness far away from the injection gate. However, higher impact resistance values are found in samples tested in MD direction located at the extreme positions (MD-A and MD-C). Once again, the more random fiber orientation at the middle of the part makes the impact resistance obtained in MD-B specimen equal to the average values resulted in the transversal direction (TD-B). By controlling a proper solid skin thickness and fiber orientation, it would be possible to produce lightweight products without largely sacrificing the impact properties.

Fracture behavior

Crack Tip Opening Displacement CTOD

Force-displacement curves obtained with *SENT* specimens and tested in TD direction are shown in Figure 9. In all materials, crack propagation initiated before reaching the maximum force, and before undergoing full ligament yielding. Additionally, crack propagation was not stable along the whole ligament, and there was no parallelism between curves. Therefore the Essential Work of Fracture method could not be applied for fracture characterization. The instabilities occurred during crack propagation in foamed samples prevented from an accurate characterization of fracture behavior by means of the *J-integral* technique. The size of the plastic zone in the strain fields plotted in Figure 9 does not allow the application of the Linear Elastic Fracture Mechanics theories, either. Instead, the *CTOD* parameter was determined by *Digital Image Correlation* (*DIC*) technique, whose results are displayed in Table 4. Cells acting as crack arrestors by blunting the crack tip gives rise to an increase in *CTOD* values with the foaming ratio (up to 15% in foamed samples with 10% of weight reduction and 10% in 20% of weight reduction when crack propagated in MD direction, and about 10% in the opposite direction).

In case of solid specimens, higher *CTOD* values are obtained in TD direction, which might be due to the preferential fiber orientation in the filling direction opposing crack propagation. However, the effect of fiber orientation becomes less influential when foaming, with more balanced *CTOD* values between MD and TD directions. In foamed *SENT* specimens with 20% of weight reduction, no great differences from both orientations are found. As seen before, similar cell structure was examined in both directions, and more randomly fiber orientation is suggested in that region. Thus, the diminished solid skin thickness in this second series of foamed materials could have led to this more isotropic behavior, reaching similar *CTOD* values to that of foamed samples with 10% of weight reduction tested in TD direction.

Failure mechanisms of fiber-filled polymers can be classified into matrix-related (crazing, voiding, fracture, shear yielding) and fiber-related (debonding, bridging, pull-out and fracture) [43]. Stress is concentrated at the fiber ends within the damage zone, prompting the occurrence of crazing in PP matrix, and debonding along the fiber surfaces. Then, crack propagates by connection of the different craze planes due to fiber debonding, pull-out and fracture together with matrix deformation (shear yielding and plastic deformation) [44]. Thus, fiber orientation has a remarked effect on crack propagation. Fiber aligned transversal to the crack path tends to restrict propagation and forces it to follow a zig-zag path, resulting in ductile failure, whereas fiber parallel to crack propagation direction enables brittle fracture. The occurrence of crazes degenerating in unstable crack propagation is the quasi-exclusive failure mechanisms for composites [45]. Fiber “bridging” kept both crack faces fairly close to each other, so the analysis of the crack propagation was not an easy task with this material. As a matter of fact, values of *CTOD* of PP 20GF were half the ones measured with ABS tested in the same conditions in a previous work [46].

In reference to the crack propagation process, crack propagates in solid plates in a stable manner along a straight line up to the catastrophic failure. In the foamed samples, the subsequent process of deformation, rupture and cell coalescence makes the crack propagation more unstable. The crack path is not a straight line, and secondary cracks ahead of the main crack tip can be observed (Figure 9f) and Figure 9i)). To get a better insight into the crack propagation phenomena, fracture surfaces were analyzed by *Scanning Electron Microscopy* (Figure 10). The areas near the notch with quasi-stable crack propagation shows typical ductile rough fracture surface, characterized by ridges and peaks due to material tearing. When unstable failure takes place, the corresponding areas exhibited smooth surfaces due to the brittle fracture.

As highlighted in Figure 10, the ductile-brittle behavior transition is not performed uniformly along the whole thickness of the sample, but the ductile region is more extended in the foamed core than in the solid skin. This effect could be the reason for the emergence of the secondary cracks highlighted in Figure 9. In all cases, the ligament length of stable or quasi-stable crack propagation is around 8-9 mm.

Fracture toughness K_{Ic}

The fracture toughness obtained in solid and foamed samples from high load speed tests are summarized in Table 4. Early studies on the effect of glass fiber on the fracture behavior of polymers showed an increase in fracture toughness for brittle matrix materials, but a decrease for initially ductile ones [47]. For thick samples under high loading speed, the crack tips are under plane-strain condition and brittle fracture of cell walls around crack tip is promoted [48]. Examination of fracture surfaces revealed that brittle matrix failure and fiber bridging and pull-out were the main fracture mechanisms, although fiber breakage was expected at high loading rates, decreasing toughness [19].

Due to stress concentration on cell walls, lower density and energy absorption capability, the fracture toughness decreases by around 20% and 40% with the foaming ratio (10% and 20% of weight reduction, respectively). In TD direction, solid and foamed samples taken from the extreme areas (TD-A and TD-C) present higher K_{Ic} than the central section (TD-B). From the analysis above it was observed that the middle of the plate is a region with scarcely dependence on fiber orientation, where properties in both transversal directions are almost equal (TD-B and MD-B). Similar conclusions were found by Hartl, Jerabek *et al* [49] with notched samples tooled from the center area of PP GF plates under Charpy impact tests.

Fiber orientation plays a relevant role on fracture toughness at high impact loads. Table 4 points out an increase in values of K_{Ic} in solid samples tested in MD direction as the distance from the injection gate increases, even higher than that obtained in TD direction. This might be due to the alignment of fibers in the transverse direction to filling in the core region, opposing to crack propagation. Differences in fracture toughness of foamed samples between extreme and central samples (TD-A, TD-B and TD-C) are small. In the opposite direction, lower and similar values of K_{Ic} are determined in all tested specimens (MD-A, MD-B and MD-C) for each foaming condition. In neat polymers, density arises as the main factor influencing the mechanical and fracture properties. Nevertheless, fillers play an important role on this mechanical and fracture behavior, and contribute to overcome the loss in properties due to foaming and density reduction. This fact can be observed in highly fiber oriented specimens (such as TD-A and TD-C), where similar fracture toughness is obtained for foamed samples with 10% and 20% of weight reduction levels.

CONCLUSIONS

Glass fiber-reinforced Polypropylene was injection molded into square plates under solid and foaming conditions, and their morphology, mechanical and fracture characteristics were analyzed. The material structure of the foamed parts consists of two solid skins and a foamed core. Heterogeneous nucleation induced by glass fibers is the main cell forming mechanism of the studied material. Despite the weak melt strength and semicrystalline nature of PP, the incorporation of the filler decreases the energy barrier leading to uniform cell distribution along the part.

Flexural and impact properties decrease gradually with the apparent density, although specific values remain constant for all solid and foamed samples. In terms of fracture, cells act as crack arrestors by blunting the crack tip and, thus, increase the *Crack Tip Opening Displacement* (*CTOD*) value as compared to the solid counterpart. However, the fracture toughness K_{Ic} decreased with the density of the samples. Together with apparent density, fiber orientation arises as a dominant factor on mechanical properties. From Computed Tomography analysis, a preferential alignment of fibers in the transverse direction to filling in the core was observed, as well as more random and oriented fibers in the filling direction in the surface layers and extreme positions. This led to an anisotropic behavior of the mechanical performance of the injection molded part depending on the location and testing direction, which is not hampered by foaming.

By controlling the material morphology resulted from the injection molding process, different behavior and properties can be achieved. Those locations with preferential fiber orientation tend to increase mechanical properties in the concurrent loading direction overcoming partially the loss of properties due to foaming and density reduction, as has been observed in flexural and impact characteristics. In case of fracture, fibers oriented perpendicular to crack direction oppose to its propagation and increase fracture toughness.

ACKNOWLEDGEMENTS

The CT analyses were performed in the *CORELAB* laboratory at the University of Barcelona facilities with the collaboration of the *CORELAB* staff. Simulation calculations with *Moldex 3D®* software were conducted with the support of *Aida S.L*. The authors are grateful to Ministerio de Economía y Competitividad from Spain for the *MAT 2013-40730P* and *MAT 2016-80045R* projects. J. Gómez-Monterde thanks Government of Catalonia and *Rücker Lypsa S.L.U.* for their collaboration in the *Industrial Doctorate Plan*.

REFERENCES

[1] Karian H. Handbook of Polypropylene and Polypropylene Composites, Revised and Expanded. Boca Raton: CRC Press, 2003.
[2] Witik RA, Payet J, Michaud V, Ludwig C, Månson J-AE. Assessing the life cycle costs and environmental performance of lightweight materials in automobile applications. Compos Part A-Appl S. 2011;42(11):1694-709.
[3] Velasco JI, Antunes M, Realinho V, Ardanuy M. Characterization of rigid polypropylene-based microcellular foams produced by batch foaming processes. Polym Eng Sci. 2011;51(11):2120-8.
[4] Sauceau M, Fages J, Common A, Nikitine C, Rodier E. New challenges in polymer foaming: A review of extrusion processes assisted by supercritical carbon dioxide. Prog Polym Sci. 2011;36(6):749-66.
[5] Gunkel F, Spörrer ANJ, Lim GT, Bangarusampath DS, Altstädt V. Understanding Melt Rheology and Foamability of Polypropylene-based TPO Blends. J Cell Plast. 2008;44(4):307-25.
[6] Bledzki AK, Faruk O, Kirschling H, Kühn J, Jaszkiewicz A. Microcellular polymer and composites. Part II. Properties of different types of microcellular materials. Polimery-W. 2007;52(1):3-12.
[7] Doroudiani S, Park CB, Kortschot MT. Effect of the crystallinity and morphology on the microcellular foam structure of semicrystalline polymers. Polym Eng Sci. 1996;36(21):2645-62.
[8] Demori R, de Azeredo AP, Liberman SA, Mauler RS. Evaluation of foaming polypropylene modified with ramified polymer. AIP Conf Proc. 2015;1664(1):040004.

[9] Wang L, Wan D, Qiu J, Tang T. Effects of long chain branches on the crystallization and foaming behaviors of polypropylene-g-poly(ethylene-co-1-butene) graft copolymers with well-defined molecular structures. Polymer. 2012;53(21):4737-57.
[10] Guo M-C, Heuzey M-C, Carreau PJ. Cell structure and dynamic properties of injection molded polypropylene foams. Polym Eng Sci. 2007;47(7):1070-81.
[11] Huang H-X, Wang J-K, Sun X-H. Improving of Cell Structure of Microcellular Foams Based on Polypropylene/High-density Polyethylene Blends. J Cell Plast. 2008;44(1):69-85.
[12] Leung SN, Wong A, Park CB, Zong JH. Ideal surface geometries of nucleating agents to enhance cell nucleation in polymeric foaming processes. J Appl Polym Sci. 2008;108(6):3997-4003.
[13] Mueller J, Spoerrer A, Altstaedt V. Foam injection moulding of a TPO/TPC-blend and the effect of different nucleating agents on the resulting foam structure. AIP Conf Proc. 2014;1593(1):367-73.
[14] Saiz-Arroyo C, Rodríguez-Pérez MÁ, Velasco JI, Saja JAd. Influence of foaming process on the structure–properties relationship of foamed LDPE/silica nanocomposites. Compos Part B-Eng. 2013;48:40-50.
[15] Faruk O, Bledzki AK, Matuana LM. Microcellular Foamed Wood-Plastic Composites by Different Processes: a Review. Macromol Mater Eng. 2007;292(2):113-27.
[16] Jiang M, Li H, Fang D, Liu L, Tai Q, Li L, et al. Structure–Property Relationship in Injection-Molded Polypropylene/Clay Composite Foams. Mater Manuf Processes. 2014;29(2):160-5.
[17] Zhang ZX, Sridhar V, Kim JK. Polypropylene–waste ground rubber tire powder microcellular composites: Effect of processing variables on morphology and physico-mechanical properties. Polym Composite. 2008;29(11):1276-84.
[18] Zhao H, Cui Z, Wang X, Turng L-S, Peng X. Processing and characterization of solid and microcellular poly(lactic acid)/polyhydroxybutyrate-valerate (PLA/PHBV) blends and PLA/PHBV/Clay nanocomposites. Compos Part B-Eng. 2013;51:79-91.
[19] De SK, White JR. Short Fibre–Polymer Composites. Cambridge: Woodhead Publishing, 1996.
[20] Xi Z, Sha X, Liu T, Zhao L. Microcellular injection molding of polypropylene and glass fiber composites with supercritical nitrogen. J Cell Plast. 2014;50(5):489-505.
[21] Benevolenski O, Karger-Kocsis J. Fracture and failure behavior of partially consolidated discontinuous glass fiber mat-reinforced polypropylene composites (Azdel SuperLite®). Macromolecular Symposia. 2001;170(1):165-80.
[22] Monami A, Langer B, Sadilek J, Kucera J, Grellmann W. Fracture Mechanics Properties of Polymorphic Polypropylene. Procedia Materials Science. 2014;3(Supplement C):276-81.
[23] Martinez AB, Gamez-Perez J, Sanchez-Soto M, Velasco JI, Santana OO, Ll Maspoch M. The Essential Work of Fracture (EWF) method – Analyzing the Post-Yielding Fracture Mechanics of polymers. Eng Fail Anal. 2009;16(8):2604-17.
[24] Arencón D, Antunes M, Realinho V, Velasco JI. Influence of chemical nature, expansion ratio and cellular morphology on the fracture behaviour of flexible polyolefin-based foams assessed by the Essential Work of Fracture (EWF). Polym Test. 2015;43:163-72.
[25] Bárány T, Czigány T, Karger-Kocsis J. Application of the essential work of fracture (EWF) concept for polymers, related blends and composites: A review. Prog Polym Sci. 2010;35(10):1257-87.
[26] Okolieocha C, Raps D, Subramaniam K, Altstädt V. Microcellular to nanocellular polymer foams: Progress (2004–2015) and future directions – A review. Eur Polym J. 2015;73:500-19.
[27] Anderson TL. Fracture mechanics: fundamentals and applications. Boca Raton (USA): CRC press, 2005.
[28] Moore DR, Williams JG, Pavan A. Fracture mechanics testing methods for polymers, adhesives and composites. Oxford: Elsevier, ESIS Publication, 2001.
[29] Saiz-Arroyo C, de Saja JA, Velasco JI, Rodríguez-Pérez MÁ. Moulded polypropylene foams produced using chemical or physical blowing agents: structure–properties relationship. J Mater Sci. 2012;47(15):5680-92.

[30] Jiang X-L, Liu T, Xu Z-M, Zhao L, Hu G-H, Yuan W-K. Effects of crystal structure on the foaming of isotactic polypropylene using supercritical carbon dioxide as a foaming agent. J Supercrit Fluids. 2009;48(2):167-75.
[31] Colton JS, Suh NP. The nucleation of microcellular thermoplastic foam with additives: Part I: Theoretical considerations. Polym Eng Sci. 1987;27(7):485-92.
[32] Huszar M, Belblidia F, Davies HM, Arnold C, Bould D, Sienz J. Sustainable injection moulding: The impact of materials selection and gate location on part warpage and injection pressure. Sustainable Mater Technol. 2015;5:1-8.
[33] Crowson RJ, Folkes MJ, Bright PF. Rheology of short glass fiber-reinforced thermoplastics and its application to injection molding I. Fiber motion and viscosity measurement. Polym Eng Sci. 1980;20(14):925-33.
[34] Kamal MR, Song L, Singh P. Measurement of fiber and matrix orientations in fiber reinforced composites. Polym Composite. 1986;7(5):323-9.
[35] Kim EG, Park JK, Jo SH. A study on fiber orientation during the injection molding of fiber-reinforced polymeric composites: (Comparison between image processing results and numerical simulation). J Mater Process Technol. 2001;111(1–3):225-32.
[36] Gong W, He Y, Zhang C, Zhu JH, He L. Effects of Process Conditions on Mechanics Properties of Micro-Foaming PP/GF Composites. Appl Mech Mater. 2012;117-119:256-61.
[37] Mortazavian S, Fatemi A. Effects of fiber orientation and anisotropy on tensile strength and elastic modulus of short fiber reinforced polymer composites. Compos Part B-Eng. 2015;72:116-29.
[38] Lou CW, Lin CW, Hsing WH, Chen JM, Ke CY, Lin JH. Manufacturing Technique and Property Evaluation of Impact-Resistant Polypropylene/Glass Fiber Composites. Adv Mat Res. 2011;239-242:1976-9.
[39] Thomason JL. The influence of fibre length and concentration on the properties of glass fibre reinforced polypropylene: 5. Injection moulded long and short fibre PP. Compos Part A-Appl S. 2002;33(12):1641-52.
[40] Yu B, Geng C, Zhou M, Bai H, Fu Q, He B. Impact toughness of polypropylene/glass fiber composites: Interplay between intrinsic toughening and extrinsic toughening. Compos Part B-Eng. 2016;92:413-9.
[41] Akay M, Barkley D. Processing-structure-property interaction in injection moulded glass-fibre reinforced polypropylene. Compos Struct. 1985;3(3):269-93.
[42] Li M, Cao X, Luo Y. Cell structure and impact properties of foamed polystyrene in constrained conditions using supercritical carbon dioxide. Iran Polym J. 2014;23(10):775-81.
[43] Reid SR, Zhou G. Impact Behaviour of Fibre-Reinforced Composite Materials and Structures. Boca Raton: CRC Press, 2000.
[44] Karger-Kocsis J. Polypropylene: Structure, Blends and Composites. Volume 3: Composites. Dordrecht: Springer Netherlands, 1994.
[45] Tancrez J-P, Pabiot J, Rietsch F. Damage and fracture mechanisms in thermoplastic-matrix composites in relation to processing and structural parameters. Compos Sci Technol. 1996;56(7):725-31.
[46] Gómez-Monterde J, Schulte M, Ilijevic S, Hain J, Sánchez-Soto M, Santana OO, et al. Effect of microcellular foaming on the fracture behavior of ABS polymer. J Appl Polym Sci. 2016;133(7):43010.
[47] Fu S-Y, Lauke B, Mai Y-W. Science and Engineering of Short Fibre Reinforced Polymer Composites. Cambridge: Woodhead Publishing, 2009.
[48] Poapongsakorn P, Kanchanomai C. Effects of time and stress state on fracture of closed-cell PVC foam. J Sandw Struct Mater. 2012;14(5):557-71.
[49] Hartl AM, Jerabek M, Lang RW. Effect of fiber orientation, stress state and notch radius on the impact properties of short glass fiber reinforced polypropylene. Polym Test. 2015;43:1-9.

FIGURE CAPTIONS

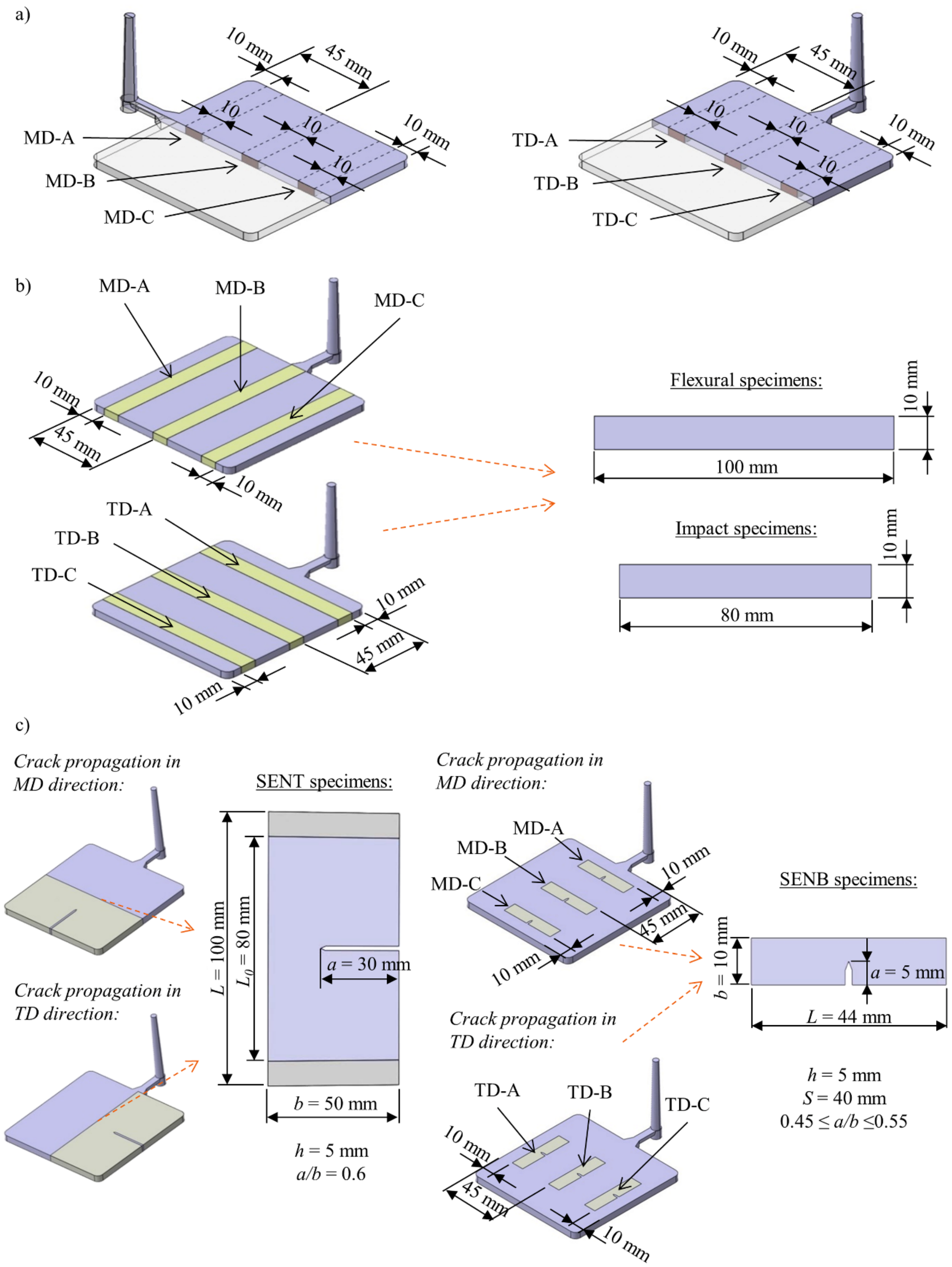

Figure 1. Schematic representation of samples extracted for a) morphological visualizations; b) mechanical characterization; c) fracture characterization.

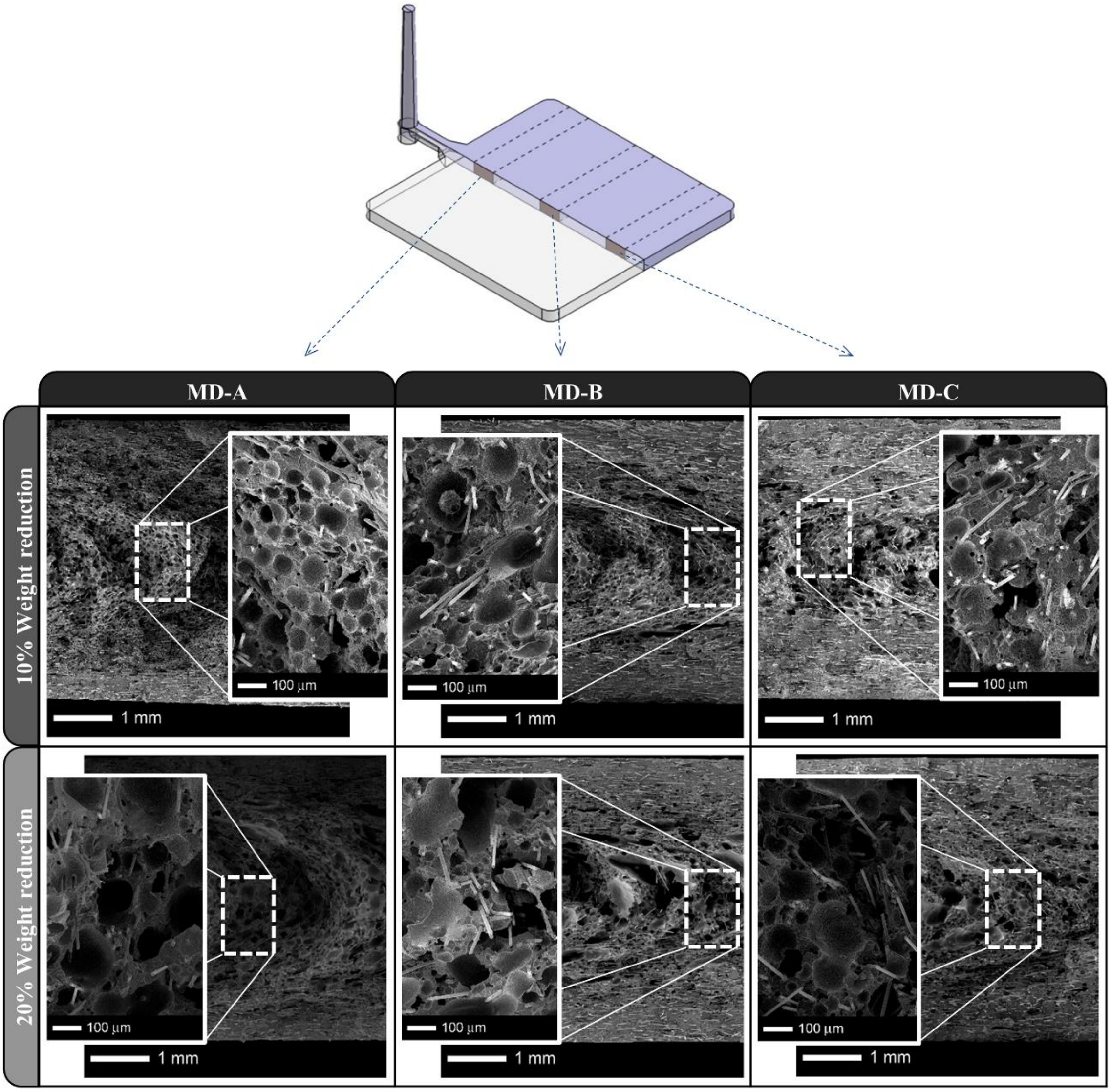

Figure 2. SEM micrographs of PP 20GF foamed plates taken in MD direction.

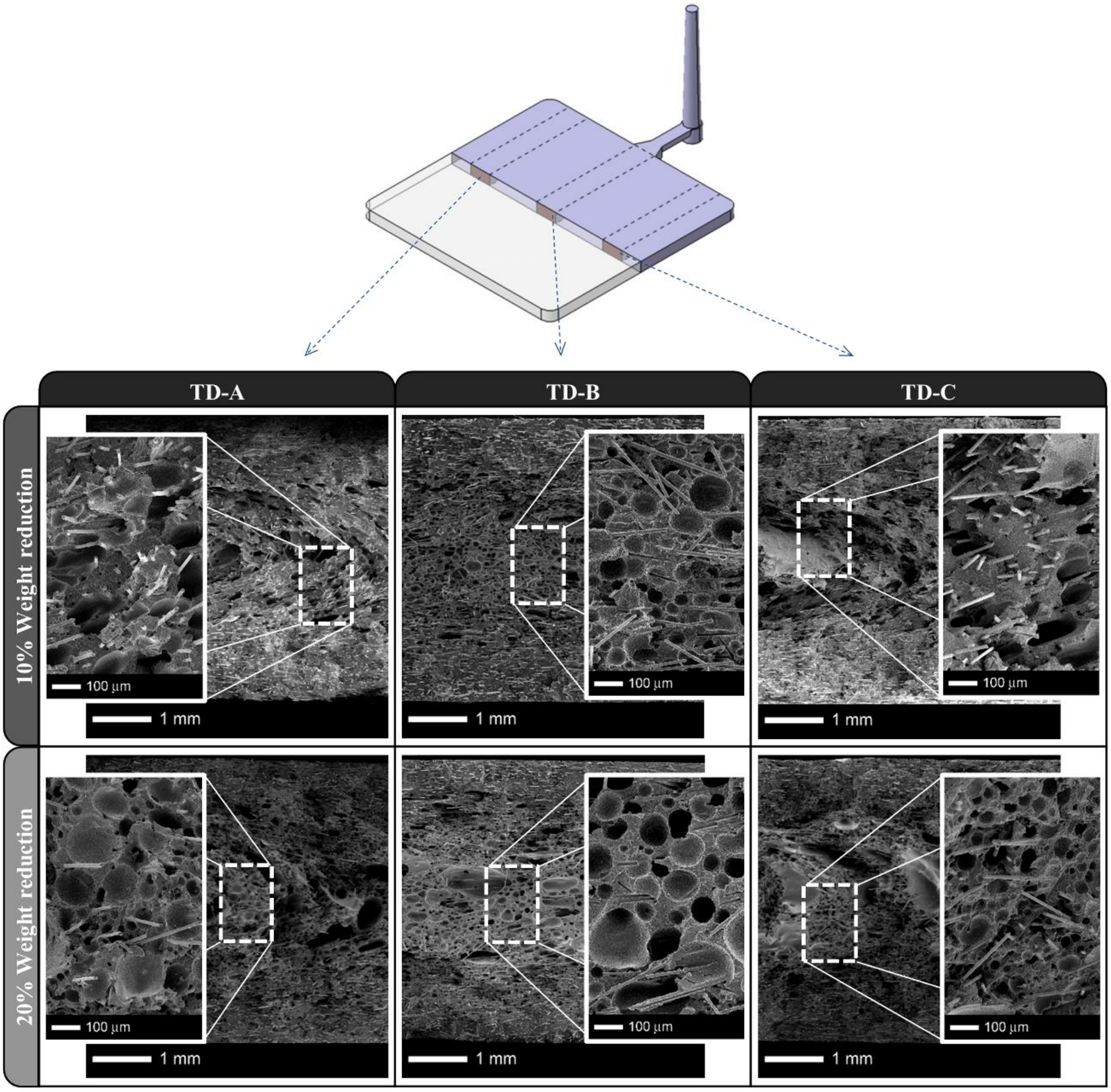

Figure 3. SEM micrographs of PP 20GF foamed plates taken in TD direction.

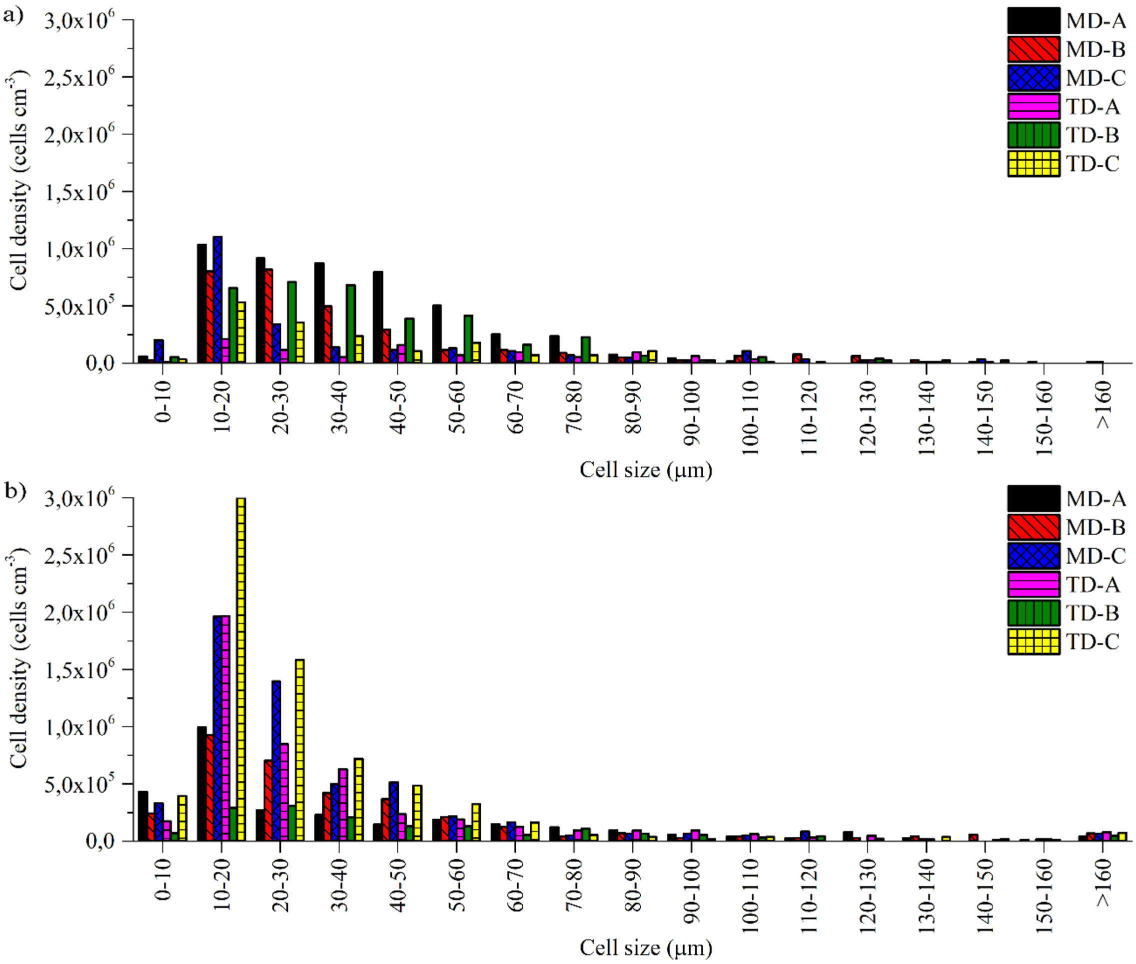

Figure 4. Cell size distribution of different sections of PP 20GF foamed samples with a) 10% weight reduction; b) 20% weight reduction.

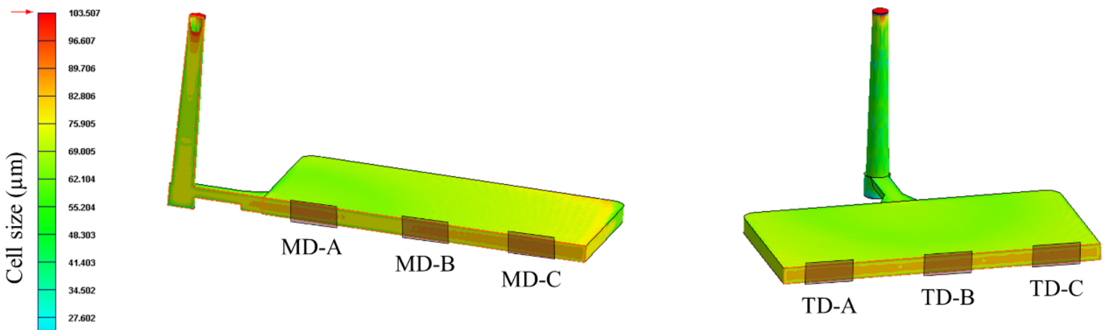

	Cell size (µm)		Cell density (cells cm^{-3})	
	10% wt. red.	**20% wt. red.**	**10% wt. red.**	**20% wt. red.**
MD-A	82	82	$1.3\cdot10^{6}$	$1.5\cdot10^{6}$
MD-B	84	80	$1.4\cdot10^{6}$	$1.6\cdot10^{6}$
MD-C	86	79	$1.3\cdot10^{6}$	$1.6\cdot10^{6}$
TD-A	87	79	$1.3\cdot10^{6}$	$1.6\cdot10^{6}$
TD-B	83	77	$1.3\cdot10^{6}$	$1.7\cdot10^{6}$
TD-C	85	79	$1.3\cdot10^{6}$	$1.6\cdot10^{6}$

Figure 5. Cell size and cell density results of PP 20GF foamed plates simulated with *Moldex 3D®* software.

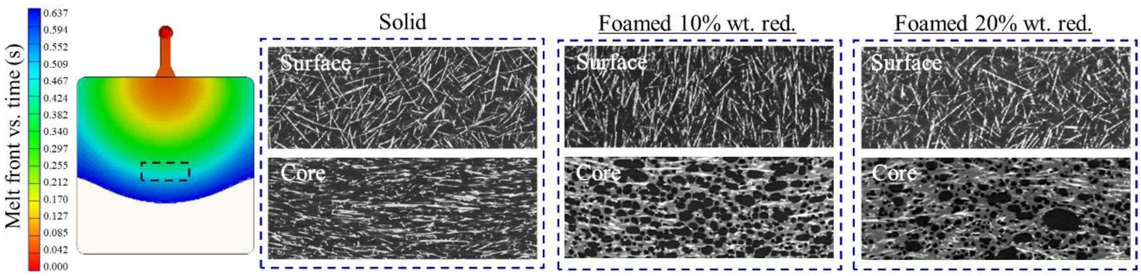

Figure 6. Filling flow pattern (melt front vs. time) and *Computed Tomography* (CT) pictures of solid and foamed PP 20GF specimens, taken in the middle of the plates indicated by the dashed rectangle.

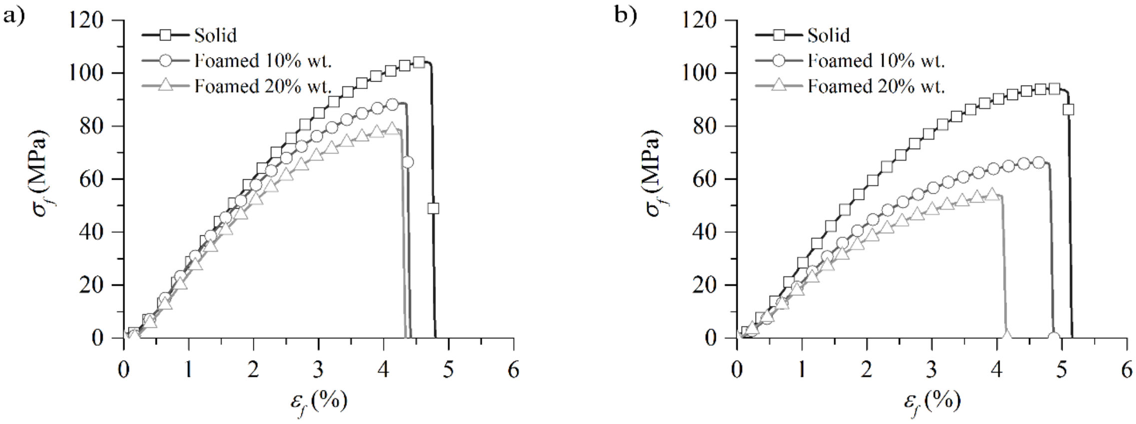

Figure 7. Flexural stress-strain curves of PP 20GF solid and foamed samples tested in a) MD; b) TD directions.

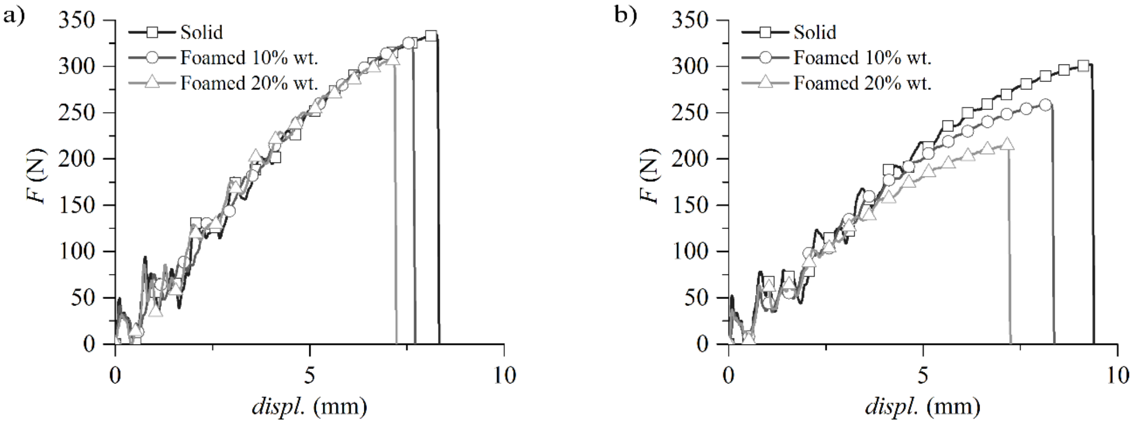

Figure 8. Impact force-displacement curves of PP 20GF samples tested in a) MD; b) TD directions.

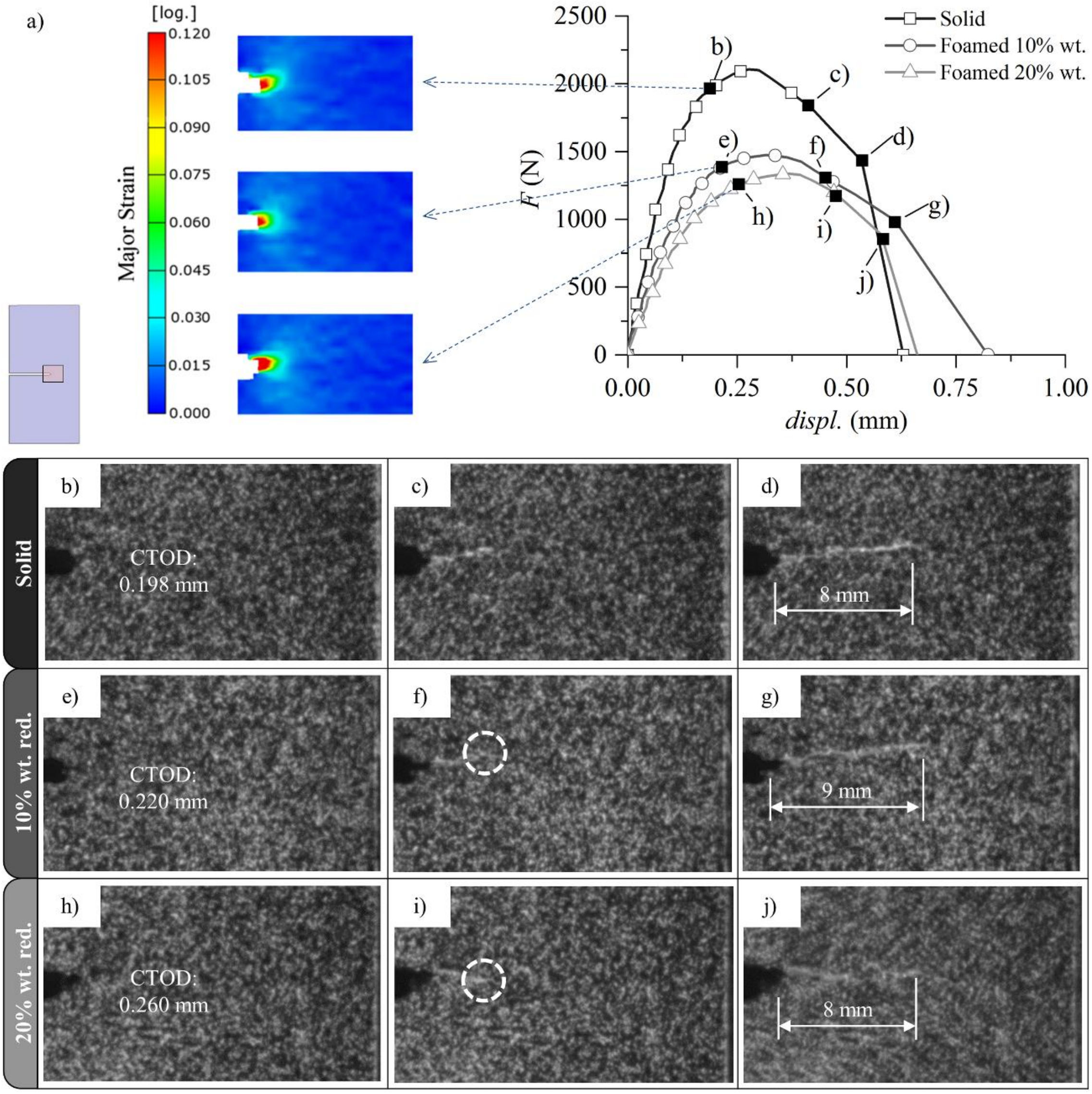

Figure 9. a) Strain field ahead of the crack tip at the crack propagation onset and force-displacement curves for solid and foamed samples tested in TD direction at 16 mm min^{-1}; b), e), h) Micrographs taken at the crack propagation onset with the corresponding *CTOD* value; c) Stable crack propagation of solid samples; f), i) quasi-stable crack propagation of foamed samples with secondary cracks ahead of the main crack front, indicated into the white dashed circles; The stable crack propagation length is indicated in figures d), g), j) for each material investigated before the catastrophic crack propagation.

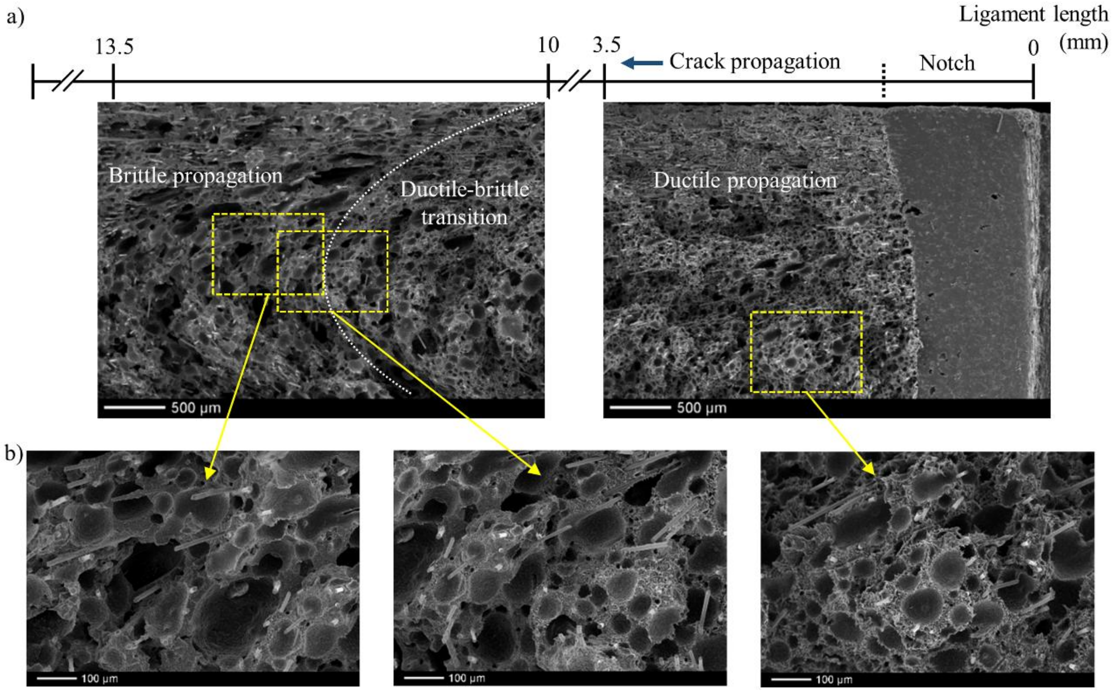

Figure 10. a) General overview of fracture surface in different ligament regions of a foamed *SENT* sample with 10% of weight reduction tested in MD direction; b) Details of different crack propagation modes.

TABLES

Table 1. Morphological parameters and apparent density of PP 20GF foamed plates.

Condition No.	Section	Density ($g\ cm^{-3}$)	Fiber content (%)	Skin thickness (mm)	Cell density ($cells\ cm^{-3}$)	Cell size (µm)
Foamed 10% wt. red.	MD-A	0.79 ± 0.01	20.3 ± 0.2	0.52	$4.8 \cdot 10^{6}$	2-100
	MD-B	0.82 ± 0.01	20.6 ± 0.1	0.71	$3.1 \cdot 10^{6}$	8-188
	MD-C	0.88 ± 0.01	20.6 ± 0.1	0.81	$2.5 \cdot 10^{6}$	6-180
	TD-A	0.86 ± 0.01	20.6 ± 0.1	0.77	$1.0 \cdot 10^{6}$	9-147
	TD-B	0.82 ± 0.01	20.6 ± 0.1	0.76	$3.5 \cdot 10^{6}$	6-135
	TD-C	0.86 ± 0.01	20.4 ± 0.1	0.77	$1.8 \cdot 10^{6}$	3-145
Foamed 20% wt. red.	MD-A	0.67 ± 0.01	20.5 ± 0.3	0.42	$2.9 \cdot 10^{6}$	7-252
	MD-B	0.73 ± 0.01	20.3 ± 0.3	0.59	$3.4 \cdot 10^{6}$	4-240
	MD-C	0.80 ± 0.01	20.5 ± 0.1	0.71	$5.5 \cdot 10^{6}$	7-203
	TD-A	0.78 ± 0.01	20.2 ± 0.4	0.59	$4.7 \cdot 10^{6}$	7-243
	TD-B	0.73 ± 0.01	20.3 ± 0.3	0.58	$1.6 \cdot 10^{6}$	2-248
	TD-C	0.78 ± 0.01	20.2 ± 0.2	0.59	$7.0 \cdot 10^{6}$	6-215

Table 2. Flexural properties in different sections of PP 20GF square plates.

Condition No.	**Section**	E_f **(MPa)**	σ_f **(MPa)**	E_f/ρ **(MPa/g cm^{-3})**	σ_f/ρ **(MPa/g cm^{-3})**
Solid	MD-A	3851 ± 41	102.0 ± 1.6	3739 ± 52	99.1 ± 1.0
	MD-B	3267 ± 52	79.4 ± 2.4	3194 ± 50	77.6 ± 1.5
	MD-C	3903 ± 61	102.8 ± 2.0	3834 ± 99	100.9 ± 1.2
	TD-A	3138 ± 88	87.0 ± 2.4	3049 ± 54	84.5 ± 1.9
	TD-B	3002 ± 76	86.6 ± 1.0	2870 ± 88	82.9 ± 1.3
	TD-C	3196 ± 90	91.6 ± 2.2	3084 ± 62	88.4 ± 1.3
Foamed 10% wt. red.	MD-A	3702 ± 59	88.8 ± 1.0	4181 ± 59	100.3 ± 1.3
	MD-B	2888 ± 68	66.6 ± 0.6	3469 ± 50	80.0 ± 0.5
	MD-C	3614 ± 91	87.8 ± 2.6	4062 ± 68	98.6 ± 2.2
	TD-A	2500 ± 81	65.5 ± 0.4	3002 ± 100	78.7 ± 1.1
	TD-B	2333 ± 85	60.9 ± 0.9	2699 ± 90	70.5 ± 0.8
	TD-C	2595 ± 83	66.3 ± 1.1	2806 ± 75	71.7 ± 0.4
Foamed 20% wt. red.	MD-A	3287 ± 56	78.8 ± 1.0	4151 ± 70	99.5 ± 1.7
	MD-B	2530 ± 47	59.0 ± 0.7	3441 ± 58	80.2 ± 0.9
	MD-C	3205 ± 33	76.8 ± 1.1	4030 ± 55	96.6 ± 1.5
	TD-A	2062 ± 41	52.2 ± 0.9	2810 ± 58	71.1 ± 1.2
	TD-B	2038 ± 88	50.6 ± 2.3	2572 ± 99	63.8 ± 2.5
	TD-C	2266 ± 49	55.6 ± 2.4	2762 ± 65	67.8 ± 2.9

Table 3. Impact resistance determined in different sections of PP 20GF square plates.

Condition No.	**Section**	a_{cU} (kJ m^{-2})	a_{cU}/ρ (kJ m^{-2}/g cm^{-3})
Solid	MD-A	31.0 ± 2.7	30.4 ± 2.8
	MD-B	24.0 ± 2.2	23.5 ± 2.5
	MD-C	29.9 ± 1.8	29.2 ± 2.0
	TD-A	32.3 ± 1.9	31.8 ± 2.3
	TD-B	30.6 ± 0.3	30.1 ± 0.6
	TD-C	28.2 ± 1.8	27.8 ± 2.1
Foamed 10% wt. red.	MD-A	25.9 ± 1.3	29.5 ± 1.7
	MD-B	18.5 ± 0.7	22.4 ± 1.1
	MD-C	25.4 ± 1.7	29.0 ± 2.1
	TD-A	21.1 ± 1.8	26.4 ± 2.5
	TD-B	20.9 ± 1.5	24.8 ± 2.0
	TD-C	21.9 ± 1.3	24.1 ± 1.7
Foamed 20% wt. red.	MD-A	23.2 ± 0.8	29.7 ± 1.2
	MD-B	15.5 ± 1.0	21.3 ± 1.5
	MD-C	23.0 ± 1.2	28.9 ± 1.8
	TD-A	16.2 ± 1.2	21.4 ± 1.7
	TD-B	14.7 ± 0.3	21.1 ± 0.6
	TD-C	16.2 ± 1.4	20.2 ± 2.0

Table 4. *CTOD* and K_{Ic} fracture parameters of PP 20GF square plates.

Condition No.	**Section**	***CTOD* (mm)**	**K_{Ic} (MPa $m^{-1/2}$)**
Solid	MD-A	-	3.52 ± 0.14
	MD-B	0.194 ± 0.011	3.95 ± 0.15
	MD-C	-	4.44 ± 0.13
	TD-A	-	4.02 ± 0.19
	TD-B	0.226 ± 0.020	3.06 ± 0.14
	TD-C	-	3.47 ± 0.22
Foamed 10% wt. red.	MD-A	-	2.80 ± 0.16
	MD-B	0.229 ± 0.008	2.41 ± 0.18
	MD-C	-	2.88 ± 0.13
	TD-A	-	2.86 ± 0.15
	TD-B	0.249 ± 0.020	2.32 ± 0.18
	TD-C	-	2.54 ± 0.16
Foamed 20% wt. red.	MD-A	-	1.84 ± 0.18
	MD-B	0.254 ± 0.014	1.84 ± 0.18
	MD-C	-	1.92 ± 0.05
	TD-A	-	2.84 ± 0.16
	TD-B	0.251 ± 0.020	1.59 ± 0.12
	TD-C	-	2.41 ± 0.07

Figure 1
Click here to download high resolution image

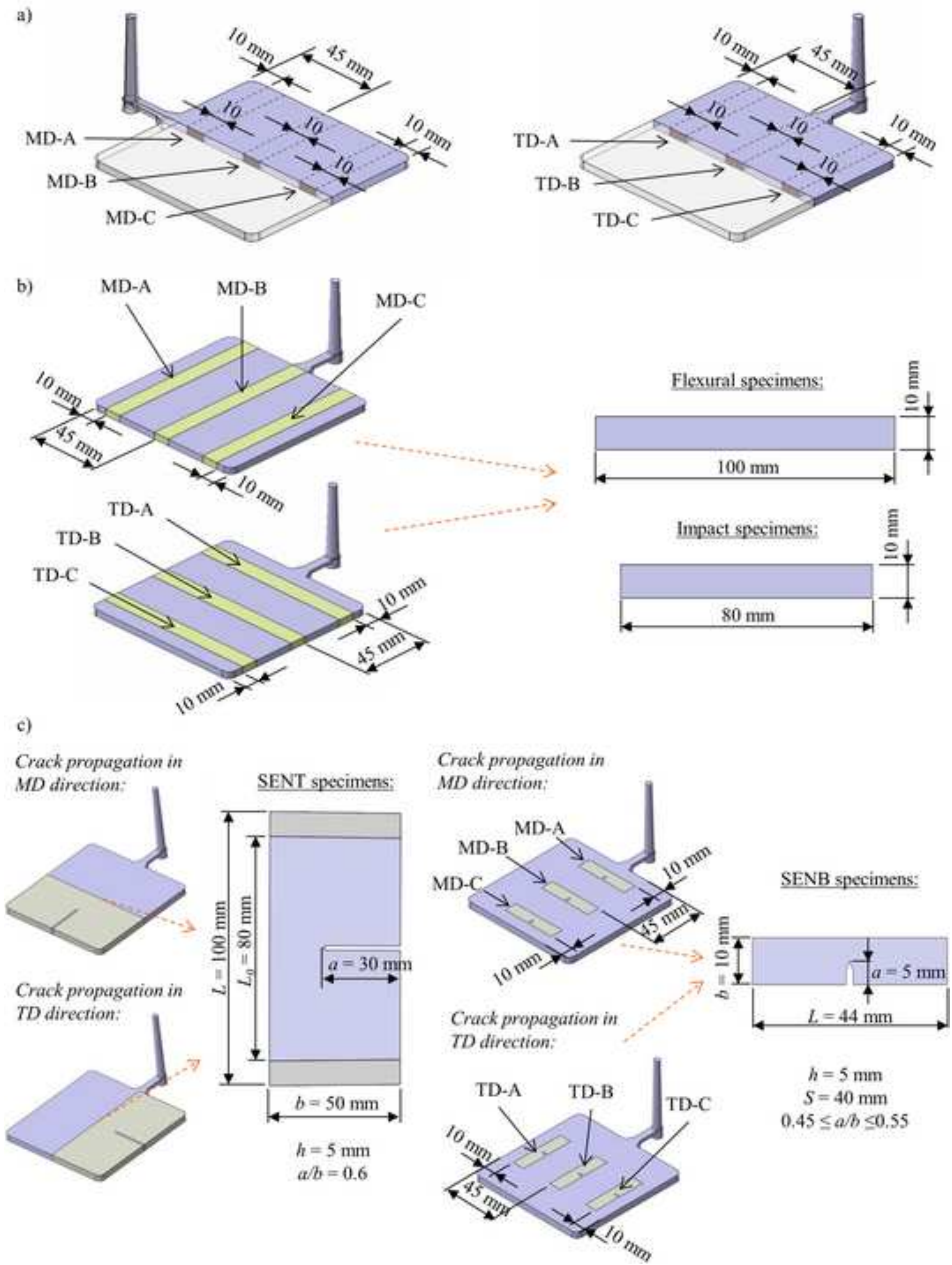

Figure 2
Click here to download high resolution image

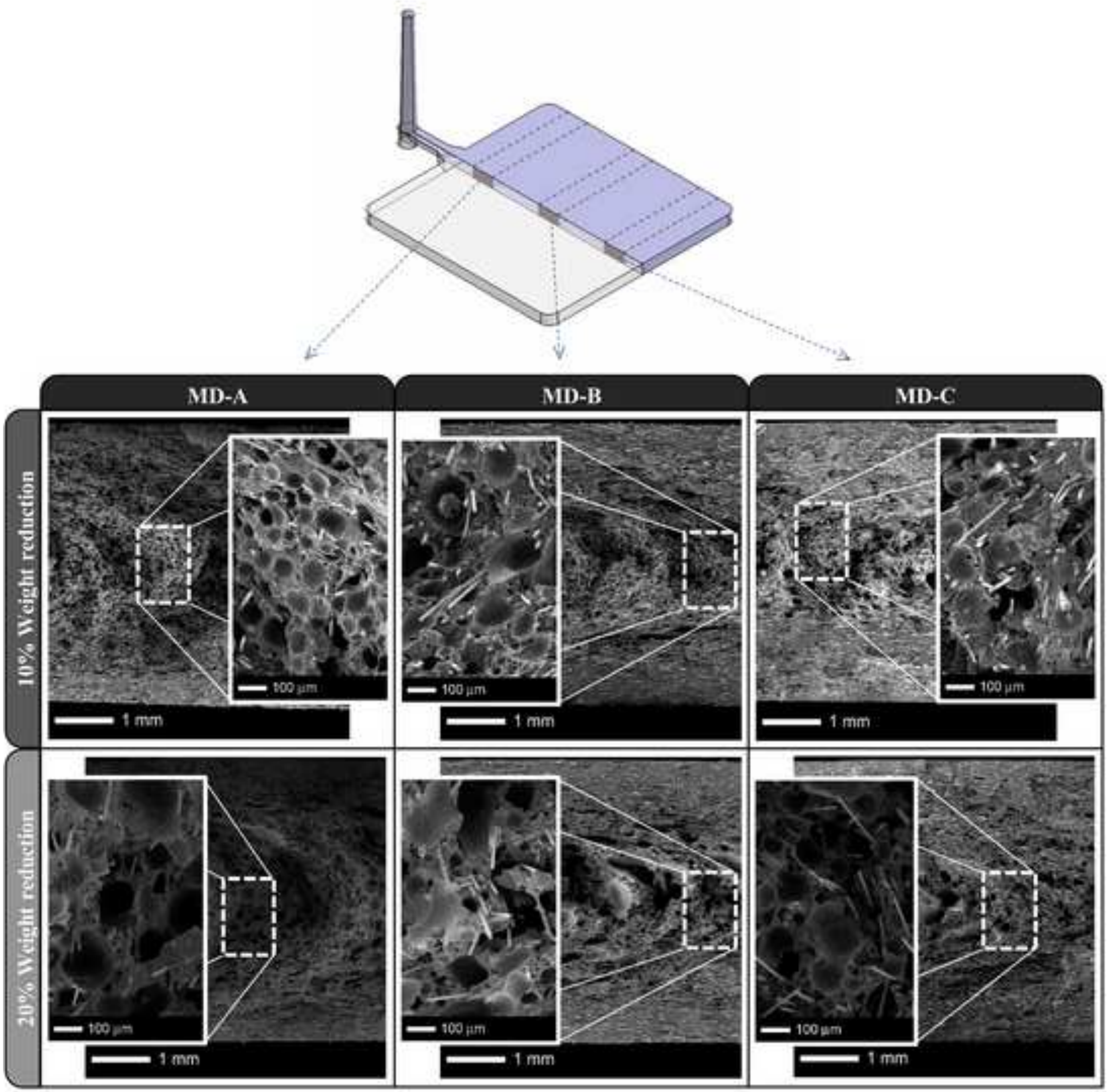

Figure 3
Click here to download high resolution image

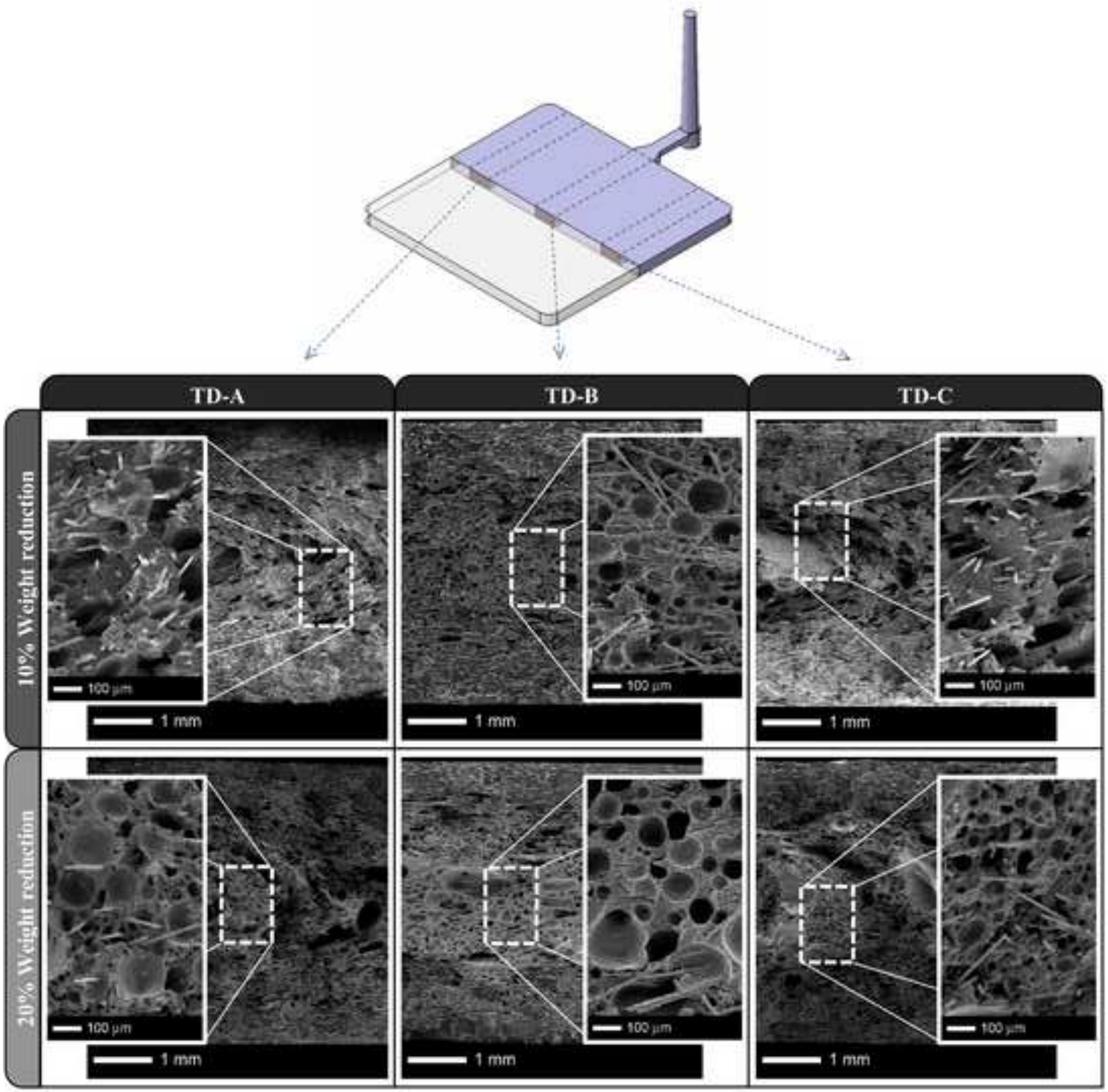

Figure 4
Click here to download high resolution image

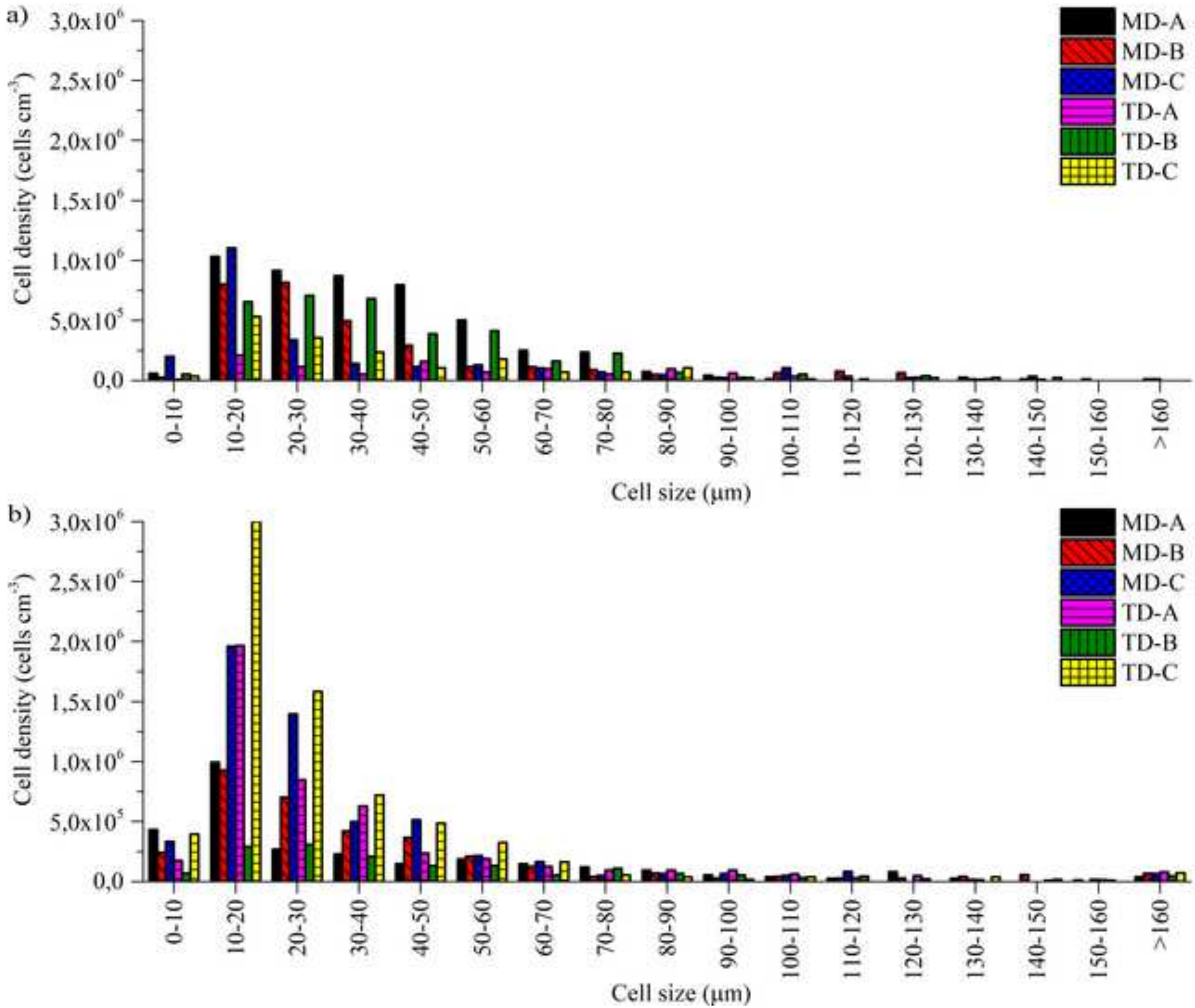

Figure 5

Click here to download high resolution image

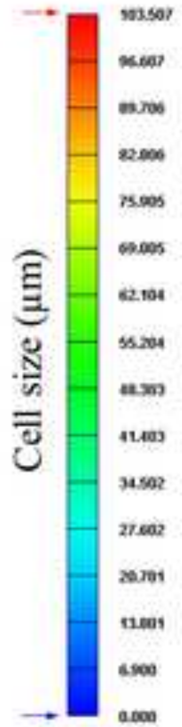

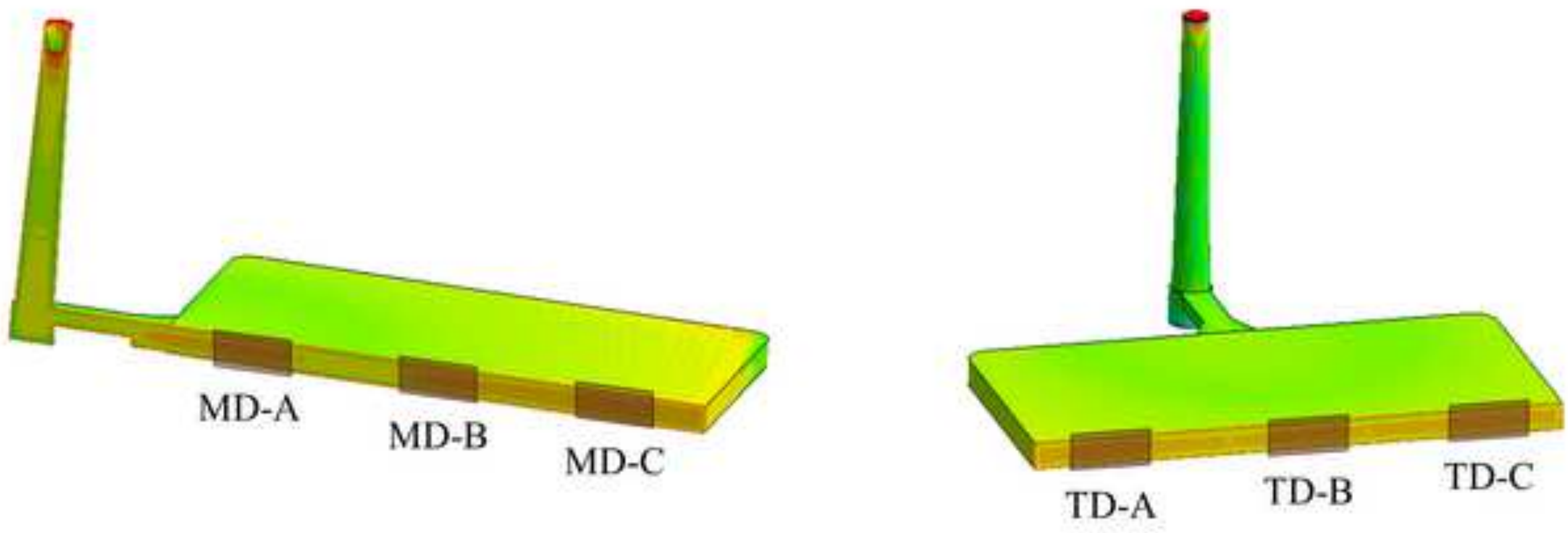

	Cell size (µm)		Cell density (cells cm^{-3})	
	10% wt. red.	20% wt. red.	10% wt. red.	20% wt. red.
MD-A	82	82	$1.3 \cdot 10^6$	$1.5 \cdot 10^6$
MD-B	84	80	$1.4 \cdot 10^6$	$1.6 \cdot 10^6$
MD-C	86	79	$1.3 \cdot 10^6$	$1.6 \cdot 10^6$
TD-A	87	79	$1.3 \cdot 10^6$	$1.6 \cdot 10^6$
TD-B	83	77	$1.3 \cdot 10^6$	$1.7 \cdot 10^6$
TD-C	85	79	$1.3 \cdot 10^6$	$1.6 \cdot 10^6$

Figure 6
Click here to download high resolution image

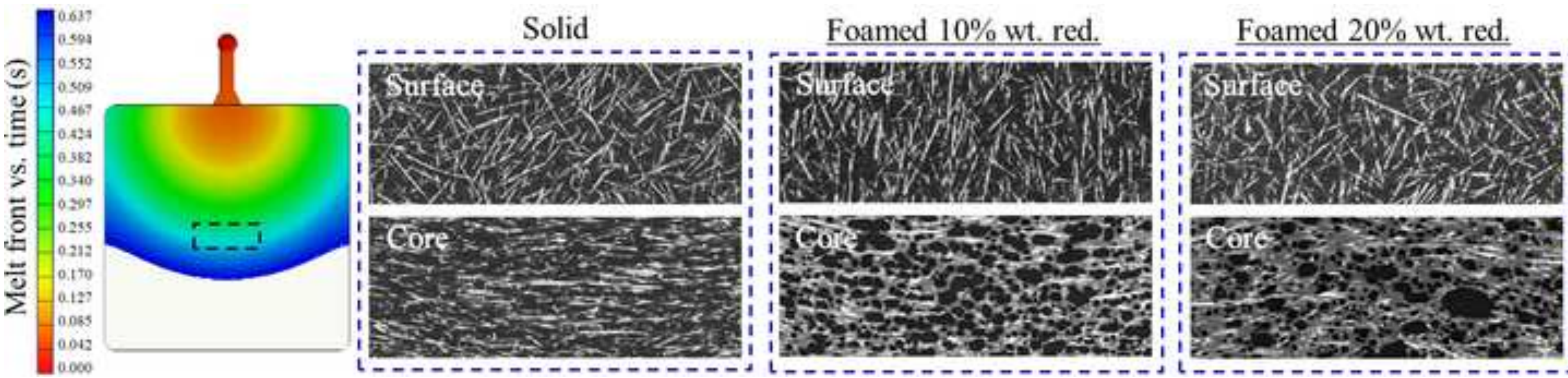

Figure 7
Click here to download high resolution image

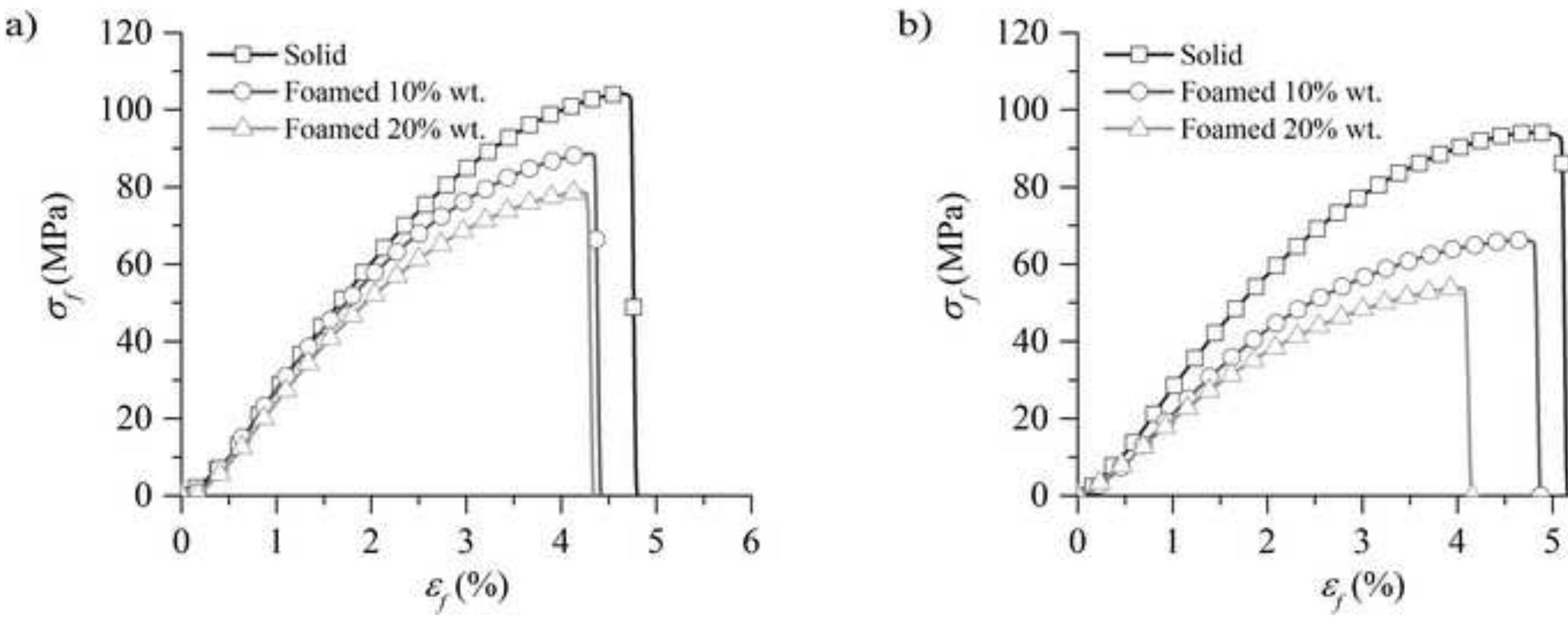

Figure 8
Click here to download high resolution image

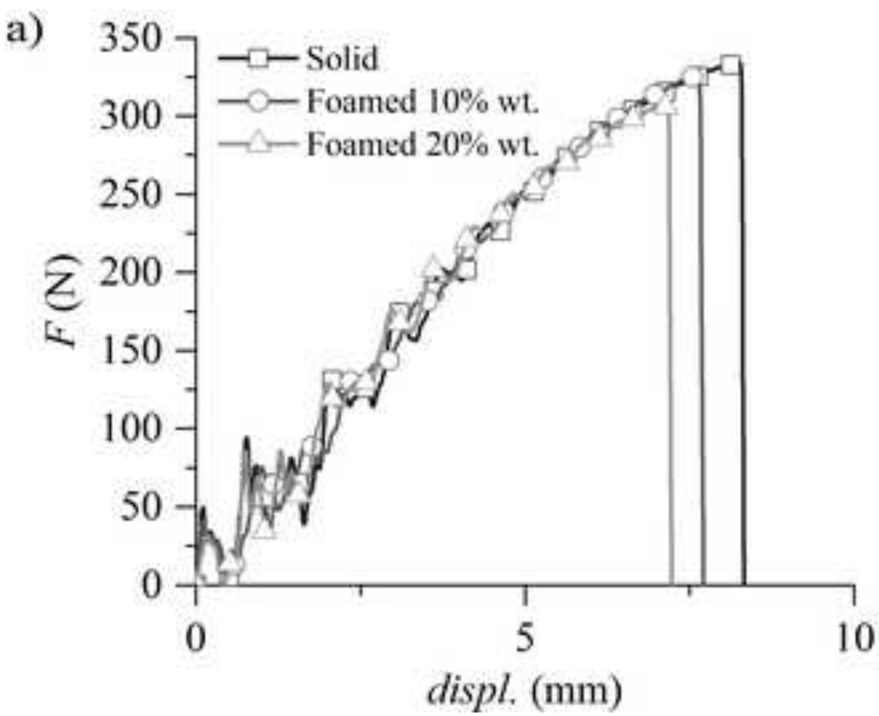

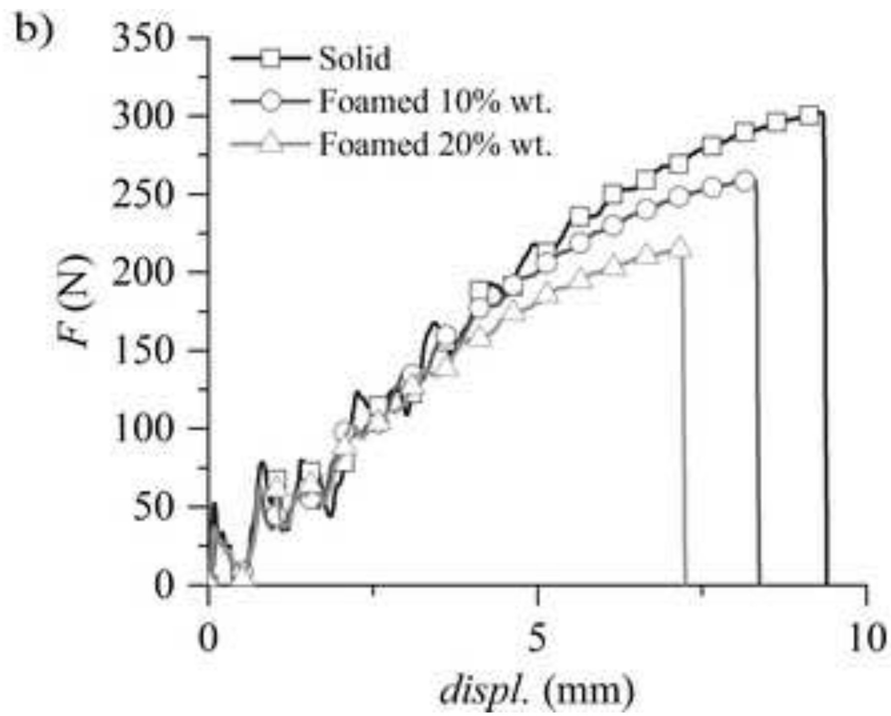

Figure 9

Click here to download high resolution image

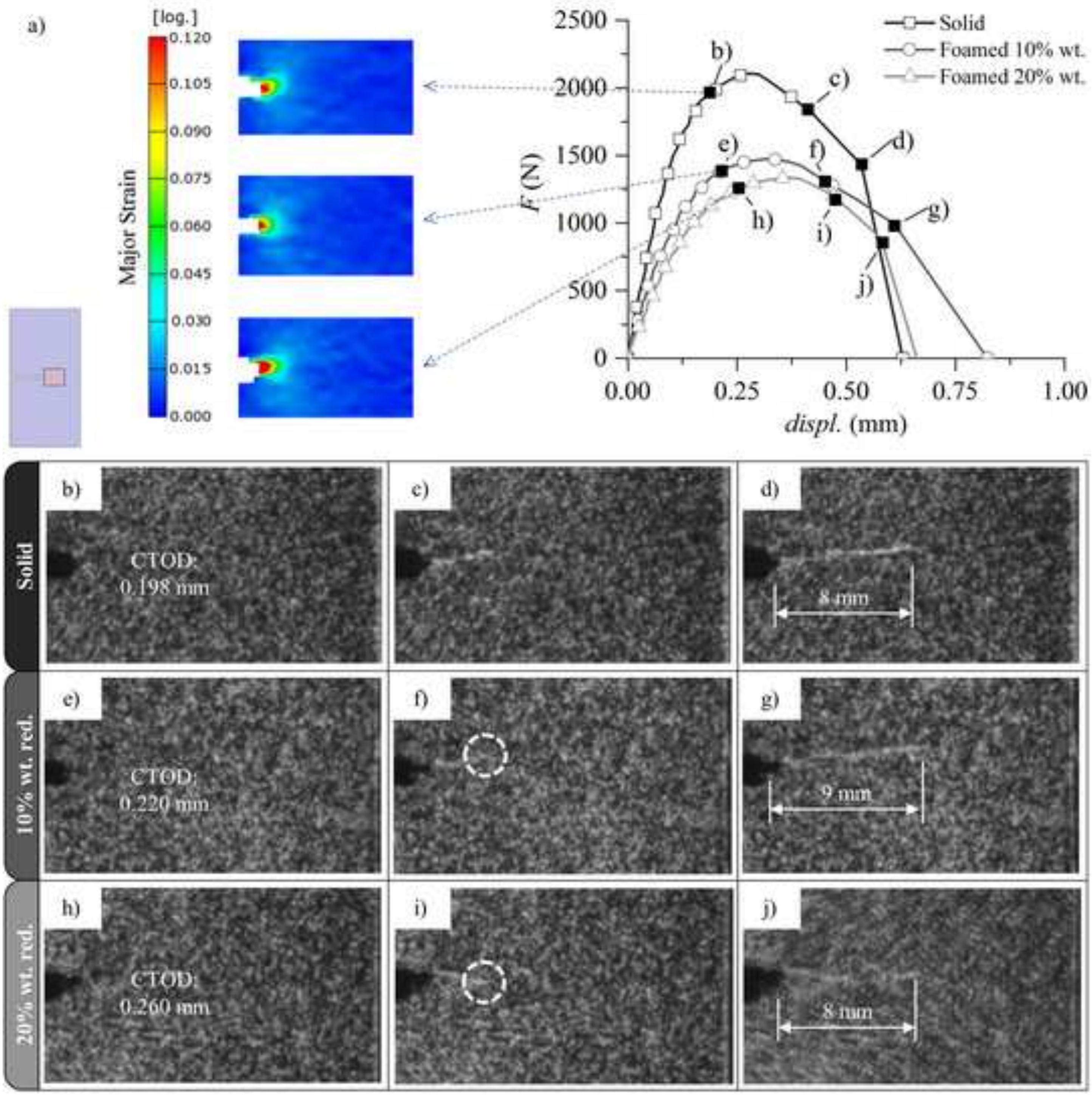

Figure 10

Click here to download high resolution image